

See discussions, stats, and author profiles for this publication at: <https://www.researchgate.net/publication/265335278>

# Multiscale Particle-Based Modeling of Flowing Platelets in Blood Plasma Using Dissipative Particle Dynamics and Coarse Grained Molecular Dynamics

ARTICLE *in* CELLULAR AND MOLECULAR BIOENGINEERING · DECEMBER 2014

Impact Factor: 1.32 · DOI: 10.1007/s12195-014-0356-5

---

CITATIONS

6

---

READS

133

## 6 AUTHORS, INCLUDING:



Peng Zhang

Stony Brook University

44 PUBLICATIONS 78 CITATIONS

[SEE PROFILE](#)



Na Zhang

Stony Brook University

13 PUBLICATIONS 17 CITATIONS

[SEE PROFILE](#)



Yuefan Deng

Stony Brook University

95 PUBLICATIONS 588 CITATIONS

[SEE PROFILE](#)



Danny Bluestein

Stony Brook University

195 PUBLICATIONS 2,196 CITATIONS

[SEE PROFILE](#)

# Multiscale Particle-Based Modeling of Flowing Platelets in Blood Plasma Using Dissipative Particle Dynamics and Coarse Grained Molecular Dynamics

PENG ZHANG,<sup>1</sup> CHAO GAO,<sup>1</sup> NA ZHANG,<sup>2</sup> MARVIN J. SLEPIAN,<sup>1,3</sup> YUEFAN DENG,<sup>2</sup> and DANNY BLUESTEIN<sup>1</sup>

<sup>1</sup>Department of Biomedical Engineering, HSC T15-090, Stony Brook University, Stony Brook, NY 11794-8151, USA;

<sup>2</sup>Department of Applied Mathematics and Statistics, Stony Brook University, Stony Brook, NY 11794, USA; and <sup>3</sup>Departments of Medicine and Biomedical Engineering and Sarver Heart Center, University of Arizona, Tucson, AZ 85721, USA

(Received 1 April 2014; accepted 18 August 2014)

Associate Editor Aleksander S Popel oversaw the review of this article.

**Abstract**—We developed a multiscale particle-based model of platelets, to study the transport dynamics of shear stresses between the surrounding fluid and the platelet membrane. This model facilitates a more accurate prediction of the activation potential of platelets by viscous shear stresses—one of the major mechanisms leading to thrombus formation in cardiovascular diseases and in prosthetic cardiovascular devices. The interface of the model couples coarse-grained molecular dynamics (CGMD) with dissipative particle dynamics (DPD). The CGMD handles individual platelets while the DPD models the macroscopic transport of blood plasma in vessels. A hybrid force field is formulated for establishing a functional interface between the platelet membrane and the surrounding fluid, in which the microstructural changes of platelets may respond to the extracellular viscous shear stresses transferred to them. The interaction between the two systems preserves dynamic properties of the flowing platelets, such as the flipping motion. Using this multiscale particle-based approach, we have further studied the effects of the platelet elastic modulus by comparing the action of the flow-induced shear stresses on rigid and deformable platelet models. The results indicate that neglecting the platelet deformability may overestimate the stress on the platelet membrane, which in turn may lead to erroneous predictions of the platelet activation under viscous shear flow conditions. This particle-based fluid–structure interaction multiscale model offers for the first time a computationally feasible approach for simulating deformable platelets interacting with viscous blood flow, aimed at predicting flow induced platelet activation by using a highly resolved mapping of the stress distribution on the platelet membrane under dynamic flow conditions.

**Keywords**—Multiscale simulations, Platelets, Molecular dynamics, Dissipative particle dynamics.

## INTRODUCTION

The coagulation cascade of blood may be initiated by flow-induced platelet activation, which prompts clot formation in prosthetic cardiovascular devices and arterial disease processes.<sup>5,9,74</sup> While platelet activation may be induced by biochemical agonists, high shear stresses arising from pathological flow patterns or cardiovascular devices enhance the propensity of platelets to activate and initiate coagulation pathway, leading to thrombosis.<sup>1,35,44,72</sup> The platelets undergo complex biochemical and rapid morphological changes upon activation, aggregate and adhere to blood vessel walls to form thrombi. The continuum based simulations to model this complex process treat blood as continuum and solve the Navier–Stokes equations governing viscous blood flows.<sup>69</sup> Flow stresses acting on the platelets can be represented down to the order of micrometer level by continuum models.<sup>73</sup> However, the molecular effects of adhesion and aggregation bonds are on the molecular scales. A continuum based approach such as computational fluid dynamics (CFD) may fail to capture these molecular features, including the deformable nature of platelets and their activation in the form of filopodia formation in response to flow-induced stresses.<sup>73</sup> The mesoscopic particle-based methods are recently developed to model the blood cells and the thrombosis. For example, the discrete particle dynamics algorithms are widely used for modeling the surrounding fluids,<sup>16,20</sup> the blood flows in microvessel,<sup>15</sup> the interactions of blood cells<sup>23</sup> and the thrombosis growth.<sup>22,66</sup> However, the platelets are still difficult to be modeled with complex phenomena such as the highly resolved fluid–platelet dynamic interactions and the formation of filopodia. Thus, we need to develop a state-of-the-art multiscale numerical

Address correspondence to Danny Bluestein, Department of Biomedical Engineering, HSC T15-090, Stony Brook University, Stony Brook, NY 11794-8151, USA. Electronic mail: danny.bluestein@stonybrook.edu

methodology that can bridge the gap between the macroscopic scales and the molecular scales for the platelet-mediated simulations under the high shear stress conditions such as through small gap clearances in the crevices of cardiovascular devices. A successful multiscale model of platelet in response to flow stresses should be able to simulate the molecular mechanics of the platelets combined with their macroscopic transport properties that happen at disparate scales. Departing from a single scale-based method, a multi-scale model needs to integrate several scales: starting with modeling the underlying mechanics of a bottom scale system (e.g., a single platelet) and develop an interface with a top scale system (e.g., the blood flow around the platelet) that couples the disparate scales between the two systems.<sup>14,17,73</sup> To build the multiscale modeling of deformable platelets in viscous blood flows, we employed two particle-based coarse-grained methods at the mesoscale and the nanoscale respectively.

At the mesoscale level, dissipative particle dynamics (DPD) is applied to simulate the viscous shear flows recently and such simulation by us and others reproduced benchmark flow solutions such as Couette flows and other viscous flow phenomena associated with no-slip boundary conditions, boundary layers and recirculation zones formation.<sup>19,21,26,60,66,68</sup> The viscous flow no-slip boundary condition on solid walls enclosing the DPD particles is a challenge when employing DPD to simulate viscous flows including the blood plasma. Such boundary condition should perform three functions: (1) providing impenetrability of the solid boundary to the fluid particles, (2) preventing slip of the fluid particles on the solid boundary, and (3) preventing density fluctuation of the DPD fluid near this boundary. Various methods attempted to address this challenge. The Lees–Edwards (LE) boundary condition<sup>36</sup> uses a modified periodic boundary condition, in which mirror images of a simulation box are moving at opposite velocities with respect to the simulation box. Briefly, LE creates a constant shear rate Couette flow without introducing any explicit solid wall. In addition, a frozen particle (FP) boundary condition is applied to fix DPD particles in order to form a rigid wall region. Particle reflection is applied to prevent the penetration of fluid particles into the solid wall.<sup>47,55</sup> Conservative force coefficient of wall particles is adjusted and estimated when considering a fluid particle within one cutoff distance to the wall. Additionally, a particle layer (PL) boundary condition<sup>71</sup> creates a layer of fictitious particles outside the simulation box with adjusted velocities such that a velocity profile is developing across the boundary and a correct no-slip boundary condition can be obtained on the wall, obviating the need for a

physical boundary. In the present study, we extend our previous effort of modeling 3D viscous fluid flow as described in Ref. 60. This model adapted the no-slip boundary condition in Ref. 71 to construct a general boundary condition allowing the description of any complex 3D wall enclosing the DPD fluid constructed with triangular meshes.<sup>60</sup>

At the mesoscale level, the platelet is often simplified by modeling it as an ensemble of bound particles constituting an enclosed membrane with an ellipsoid shape, neglecting the molecular effects of the intra-platelet constituents and membranous deformability.<sup>39–42,50,63</sup> For example, a rigid 3D platelet-shaped spheroid was used to study platelet flipping near a wall,<sup>39</sup> whereas quiescent platelets have a relatively oblate spheroid shape.<sup>24</sup> In a following study platelets were modeled as rigid oblate spheroid with aspect ratio of 0.25 to study flipping of adhesive platelets over a substrate.<sup>50</sup> A platelet model was further developed as a rigid 3D ellipsoid to study hydrodynamic collisions and wall effects.<sup>40,41</sup> However, these studies in Refs. 39–41,50 assumed totally rigid platelets which may cause erroneous estimations of the interaction of the platelets with the surrounding fluid.<sup>38</sup> In more recent studies that employed particle based models, to facilitate the inclusion of intra-platelet structures, a platelet was modeled as a coarse-grained 3D rigid oblate spheroid based on the subcellular element (SCE) Langevin method, represented with tens of harmonic tethered SCE, for studying platelets flipping under complex flows.<sup>63</sup> We have previously employed a coarse-grained deformable platelet DPD model that is adapted from red blood cell particle-based model<sup>48</sup> composed of 444 particles on a triangular mesh for each platelet.<sup>60</sup> In the present study, we further develop this coarse-grained model to a new fine-grained model which includes the complex internal structures (elastic membrane, cytoskeleton and cytoplasm) at the nanoscale.

At the nanoscale level, molecular dynamics (MD) is usually applied to describe the fine-grained physical interactions of atoms and biomolecules and defined by molecular mechanics force fields in the context of N-body simulations.<sup>3</sup> Traditional MD simulation approach requires a huge number of atoms and sophisticated force evaluation which is not always computationally feasible, making a purely atomic based simulation such as platelets flowing in viscous blood plasma computationally prohibitive even on the largest scale HPC clusters available nowadays.<sup>3,11</sup> Spatiotemporal averaging techniques are usually applied to the classical MD such that an effective particle represents a group of atoms for accessing longer time scale phenomena resulting in a reduced force field.<sup>12,56</sup> An effective spatiotemporal averaging procedure is very sensitive to the nature of the force

field when describing the behavior of complex biomolecular systems<sup>77</sup> and is by no means a trivial task. The choice of an appropriate functional form and parameters for a coarse-grained molecular dynamics (CGMD) model may become cumbersome.<sup>56,77</sup>

Design of a functional interface for coupling the disparate scales, such as the fluid–structure interaction (FSI) problems in the CFD simulations<sup>8,52</sup> is challenging; it requires managing the spatiotemporal exchange when the flow induced stresses result in the platelet activation—a process that involves a drastic shape change of the previously quiescent platelet, which in turn affect the hydrodynamics of the surrounding fluid. Similar FSI problems, e.g., the biomechanical properties of erythrocytes in blood flow, were previously studied using a continuum-based model.<sup>10</sup> Adopting for the first time an FSI methodology to a multiscale particle-based approach for modeling deformable platelets, the current study models a blood plasma fluid–platelet interaction which is formulated by a new hybrid force field for simulating the flow dynamics of a deformable platelet.

## MATERIALS AND METHODS

Extending on our previous efforts of modeling deformable platelets in viscous fluid flows<sup>21,60</sup> to a multiscale model, we introduce two particle-based coarse-graining methods: coarse-graining molecular dynamics (CGMD) and coarse-grained stochastic dynamics (CGSD).<sup>45</sup> As the DPD method is the only CGSD method<sup>45</sup> in this paper, we use the DPD term for better clarity. DPD is formulated at the top scale to describe the viscous flow behavior and yield a wall driven Couette flow condition. Instead of the coarse-grained platelet model previously employed,<sup>48,60</sup> CGMD is formulated at the bottom scale to enable a fine-grained description of the intra-platelet constituents including the elastic membrane and cytoskeleton structure. The elasticity of the membrane is computed by conducting numerical stretching simulations which are correlated to experimental results. A hybrid force field between the platelet and the flow systems is developed to interface the top–bottom scales and to resolve the fluid–platelet interaction when platelets flipping in the viscous flows. The development of this multiscale model is the first step towards a full multiscale particle-based approach to flow-induced platelet-mediated thrombosis composed of: (i) a macroscopic model of bulk flow; (ii) a molecular-scale model of platelets in which each single platelet undergoes microstructural changes: membranous responsive deformation and spontaneous growth of pseudopodia; (iii) the dynamic interfacing of both scales for

describing: (a) flow stress dynamically mapped to the surface membrane from (i) to (ii), and (b) platelet deformation effects brought up to the top-scale rheological regime from (ii) to (i) with the goal of developing a computationally feasible fully coupled interactive multiscale particle-based model for simulating platelets dynamics and response to viscous shear flows. To facilitate this complex behavior of platelets interaction with the flow that may lead to its activation, we present in the current study highly resolved dynamic mapping of the stress distribution on the surface of the platelet membrane—taking into account the deformable platelet mechanical properties and its flow dynamics. A detailed description of the methodology that was developed to achieve this follows.

### Top-Scale Viscous Flow Model

DPD is employed to simulate viscous shear flows, in which each effective particle interacts with surrounding particles at a prescribed cutoff radius. The motion of each particle is governed by:

$$dv_i = \frac{1}{m_i} \sum_{j \in i}^N (\mathbf{F}^C dt + \mathbf{F}^D dt + \mathbf{F}^R \sqrt{dt} + \mathbf{F}^E dt) \quad (1)$$

where  $\mathbf{F}^C = \alpha \omega^C(r_{ij}) \mathbf{e}_{ij}$ ,  $\mathbf{F}^D = -\gamma \omega^D(r_{ij})(\mathbf{e}_{ij} \cdot \mathbf{v}_{ij}) \mathbf{e}_{ij}$ ,  $\mathbf{F}^R = \sigma \omega^R(r_{ij}) \zeta_{ij} \sqrt{dt} \mathbf{e}_{ij}$ ,

$\mathbf{F}^C$ ,  $\mathbf{F}^D$  and  $\mathbf{F}^R$  are the conservative, dissipative and random forces acting on the particle and  $\mathbf{F}^E$  is the external force acting on each particle to induce the fluid flow.<sup>26,37</sup>  $r_{ij}$  is the inter-particle distance,  $\mathbf{v}_{ij} = \mathbf{v}_i - \mathbf{v}_j$  and  $\mathbf{e}_{ij}$  is a unit vector in the direction  $\mathbf{r}_i - \mathbf{r}_j$ .  $\zeta_{ij}$  is a Gaussian random number with zero mean and unit variance.  $\alpha$  is the maximum inter-particle repulsion<sup>26</sup> given by  $\alpha = 75k_B T / \rho_f r_c$ , where  $\rho_f$  is the number density of flow particles. The weight function  $\omega^C$  is:

$$\omega^C(r_{ij}) = \begin{cases} (1 - r_{ij}/r_c), & r_{ij} < r_c \\ 0, & r_{ij} \geq r_c \end{cases} \quad (2)$$

Español *et al.*<sup>13</sup> established the relationship between the parameters  $\gamma$  and  $\sigma$  and weight functions as:  $\sigma^2 = 2\gamma k_B T$  and  $\omega^D = [\omega^R]^2$ . The viscosity of a multi-viscosity heterogeneous fluid can be controlled with the friction factor  $\gamma$ , an input parameter in DPD that characterizes the strength of the drag force between interacting particles.<sup>68</sup>

On the boundary a solid wall is built as a triangular mesh and a no-slip boundary condition is imposed on each triangle.<sup>60</sup> “Ghost” particle-layers are constructed using fluid particles as template for producing a velocity profile continuing along the boundary. Along with the boundary condition, a reflection is

introduced to confine the fluid particles in the wall. Specifically, a wall-driven Couette flow is reproduced for the top-scale model (Fig. 1) in which two opposing momenta with velocity of magnitude 4 are applied to the upper and lower walls. Periodic boundary condition (PBC) is imposed along the  $x$ - and  $z$ -dimensions. Following our previous work<sup>60</sup> which extends Willemesen *et al.*<sup>71</sup> DPD no-slip approach to complex 3D geometries such as a stenosis, we apply this no-slip condition to Couette shear flow between two flat plates, each composed of two triangular planes. Following Groot and Warren,<sup>26</sup> we select the number density of flow particles at  $\rho_f = 3$ . The local Reynolds number of the flow (based on a nominal dimension of 16  $\mu\text{m}$  with a velocity of 15 cm/s) is 2.59, but may also represent much higher Re flows. Beyond describing extreme blood flow conditions in small blood vessels in the microcirculation (flow velocities in arterioles and small arteries typically range from 5 to 45 cm/s, respectively), our model is intended to simulate the flow conditions through small gap clearances in the crevices of a much larger cardiovascular devices, in which platelet activation is a major clinical problem.<sup>2,75</sup> For example, Yun *et al.*<sup>75</sup> describe the flow in the hinge gap regions of artificial heart valves that are prone to developing thromboembolism. Alemu *et al.*<sup>2</sup> investigate the extreme flow conditions in smallest gap clearances that can help improve thrombogenic performance of mechanical heart valves.

To estimate the impact of friction factor  $\gamma$  and cutoff  $r_c$ , respectively, we start with empirical  $r_c = 1.0$  and vary the value of  $\gamma$  (Fig. 2) followed by setting a value of  $\gamma = 90$  and varying the value of  $r_c$  (Fig. 3). This demonstrated that  $\mu$  increases with the increasing  $\gamma$  or  $r_c$ . When  $\gamma$  or  $r_c$  crosses a threshold ( $\gamma > 100$  or  $r_c > 2.0$ ) the velocity profile of the flow deviates from the one expected for this type of Couette flow. Considering these factors, we established  $\gamma = 90$  and  $r_c = 1.8$ , and achieved the resultant flow viscosity of 0.98 mPa s. The normal viscosity of blood plasma is 1.1–1.3 mPa s<sup>26,34</sup> in fair agreement with our particle-based viscous flow system.

#### Bottom-Scale Deformable Platelet Model

CGMD approach is employed to build a molecular model of platelets. This platelet model involves the intra-platelet constituents including an elastoviscous bilayer membrane, a functional cytoskeleton structure and padding cytoplasm as shown in Fig. 1 and structural details in Fig. 4. The platelet model is composed of three zones: the membrane, cytoskeletal assembly and cytoplasm zones. The membrane (thickness of 300 Å) is designed as a cortical shell for representing

the stretchable peripheral zone that includes the phospholipid bilayer (100 Å) and the exterior coat (150–200 Å). It is characterized by spring-connected particles residing at the nodes of a network of triangles constructed by the 3D Delaunay triangulation method. The cytoskeletal assembly is designed for representing the actin-based structural zone. The actin cortex and radiating actin filaments functions of the structural zone are modeled by the rigid filamentous core and protrusible filament bundles respectively to resemble the spoke-like assembly. The filamentous core is constructed by uniformly distributing spring-connected particles along the edges and vertices of a 3D triangulation of a sphere with diameter 0.3  $\mu\text{m}$ . The filament bundles originating from the exterior of the filamentous core extend radially outward using spring-connected particles. The filament bundles are treated as straight spring bundles in the quiescent state. Each filament bundle is connected to the membrane *via* a few spring bonds that mimic spectrin and adducin activity<sup>28</sup> on the actin filament ends. This numerical approximation of the filaments, while not emulating the morphology at the atomistic scale, reflects the mechanical structure of the skeleton and its attachment to the membrane.<sup>28</sup> The cytoplasm represents the organelle zone and it is characterized by a swarm of homogeneous particles that interact with each other *via* nonbonded interactions. This zone is used to represent the gel-like behavior of the organelle zone and fills the void between membrane and cytoskeleton.

This platelet model is still a coarse-grained particle-based model for describing the very complex structure at the nanoscale. An idealized model of describing atomic details of platelet components such as  $\alpha$  granules and dense bodies would be computationally prohibitive, although it is more desired. A typical platelet could consist of more than 0.7 trillion atoms, roughly estimated by a mean platelet volume of  $\sim 7.1 \times 10^{-15} \text{ L}$  and the possible number of atoms contained in it as compared with a C12 atom with volume of  $1.0 \times 10^{-26} \text{ L}$ . The prohibitive computational resources are evident by two recent ACM Gordon Bell supercomputing performance records: the first conducted a simulation using 13 trillion grid points on a computer cluster of 1.6 million cores in 2013<sup>57</sup> and the second performed N-body simulations with 1.0 trillion particles in 2012 on a computer cluster of 0.66 million cores.<sup>31</sup> Hence, the CGMD approach is needed for coarse graining the complex biological structures currently.

This platelet model employs a reduced molecular-scale force field that includes the bonded (springs and angles) and nonbonded (Lennard-Jones (L-J) potential) interactions:

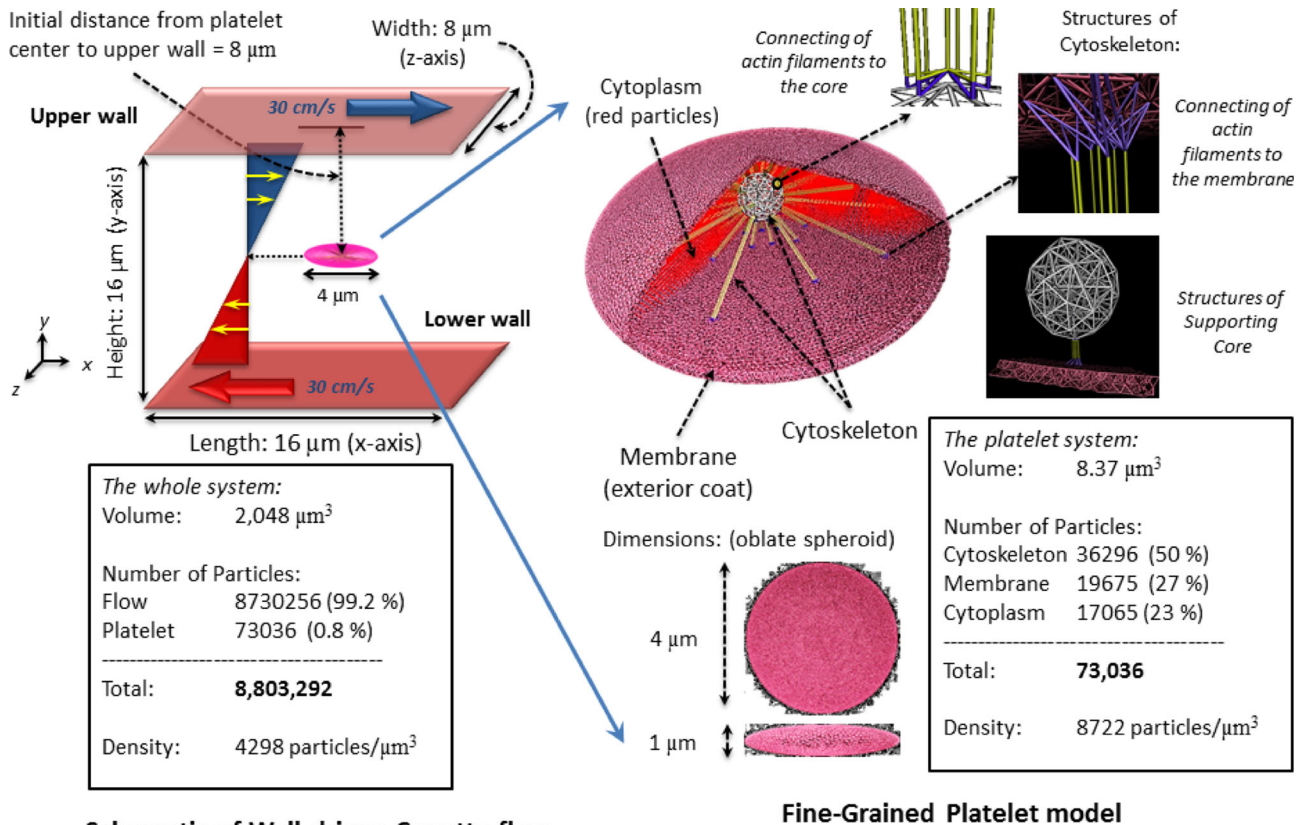


FIGURE 1. Wall-driven Couette flow and the initial position of the microscale platelet model.

$$\begin{aligned}
 E = & \sum_{\text{bonds}} k_b(r - r_0)^2 + \sum_{\text{angles}} k_\theta(\theta - \theta_0)^2 \\
 & + \sum_{\text{nonbonded pairs}} 4\epsilon \left[ \left( \frac{\sigma}{r} \right)^{12} - \left( \frac{\sigma}{r} \right)^6 \right] = E_B + E_A + E_N
 \end{aligned} \quad (3)$$

The bond energy between two adjacent filament bundle particles is given by  $k_b = 2.54 \times 10^{-4}$  kcal/mol/A<sup>2</sup> and  $r_0 = 8.0$  nm. The force constant for filament bundles is to maintain the straightness and thus to provide support to the oblate spheroid shape of quiescent platelets. The angle of a triplet of filament bundle particles is  $\theta_0 = \pi$ . This angle energy ensures that the filament bundles have strong resistance to bending or buckling. The cytoplasm particles interact with only L-J potential ( $\epsilon = 1.40 \times 10^{-20}$  kcal/mol,  $\sigma = 71.1$  nm). The L-J potential is used for imposing repulsive interactions between cytoplasm and membrane, preserving the platelet volume. Functionally, the cytoskeletal assembly and cytoplasm characterize a fine grained phenomenon of intra-platelet structures.

The membrane structure of the platelet model is allowed to deform freely. The bond energy between two adjacent membrane particles is given by  $2.54 \times 10^{-3}$  kcal/mol/A<sup>2</sup> and  $r_0 = 42.7$  nm. The area-stretch-

ing experiment is then conducted to assess the values of the membranous elasticity. The schematic experiment and the elastic responses of the membrane are illustrated in Fig. 5. The Young's modulus of human platelet membrane is reported as  $(1.7 \pm 0.6) \times 10^3$  dyn/cm<sup>2</sup> in Table 1 of Haga *et al.*<sup>27</sup> (values are mean  $\pm$  standard deviation). The Young's modulus of our membrane model is calculated as  $(1.5 \pm 0.6) \times 10^3$  dyn/cm<sup>2</sup>. Departing from these rigid models, this model characterizes the proper deforming capability of the membranous structure. This allows us to observe the responsive deformation of platelets and to investigate the dynamic stress mapping on the surface membrane upon the multiscale fluid–platelet interaction phenomena. The deformable model characterizes a membrane fluctuation or “flickering” providing the instantaneous high-frequency oscillations.<sup>18</sup> Hence, the CGMD model of platelets covers a span of nanometer scales: characteristic lengths for the filament bundles, filament core, membrane and cytoplasm are approx. 8.0, 21.3, 42.7 and 71.1 nm.

### Interfacing the Top–Bottom Scales

Combining the advantages of the highly resolved bottom scales (in the platelet system) with the less

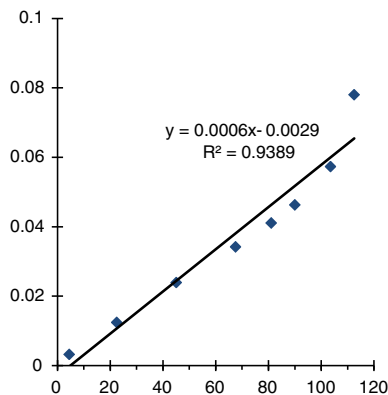


FIGURE 2. Blood plasma flow viscosity  $\mu$  (mPa s) vs. the friction factor  $\gamma$  with  $r_c = 1.0$ .

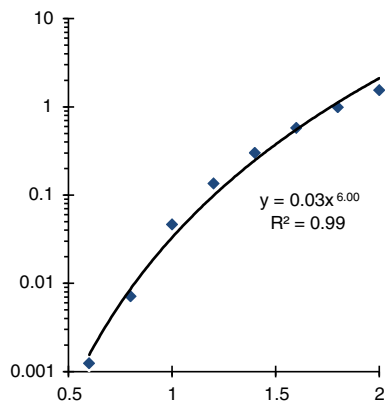


FIGURE 3. Blood plasma flow viscosity  $\mu$  (mPa s) vs. the cutoff distance  $r_c$  with  $\gamma = 90$ .

resolved top scales (in the fluid system) into a multiscale approach requires developing a force field on the boundary hybridizing the two systems.<sup>17</sup> To achieve this we develop a hybrid potential for describing the fluid–platelet interaction and then design an efficient method to parameterize this potential.<sup>64</sup> The nonbonded pairwise interparticle interaction between the top-scale flow and bottom-scale membrane particles is written as:

$$d\mathbf{v}_i = \frac{1}{m_i} \sum_{j \neq i}^N \left( \nabla U(r_{ij}) dt + \mathbf{F}^D dt + \mathbf{F}^R \sqrt{dt} \right) \quad (4)$$

where  $U(r_{ij}) = 4\epsilon_p \left[ \left( \frac{\sigma_p}{r_{ij}} \right)^{12} - \left( \frac{\sigma_p}{r_{ij}} \right)^6 \right]$ ,  $\mathbf{F}^D = -\gamma_p \omega^D(r_{ij}) (\mathbf{e}_{ij} \cdot \mathbf{v}_{ij}) \mathbf{e}_{ij}$ ,  $\mathbf{F}^R = \sigma_p \omega^R(r_{ij}) \zeta_{ij} \sqrt{dt} \mathbf{e}_{ij}$

$\epsilon_p$  and  $\sigma_p$  are the energy and length characteristic parameters in CGMD. Other parameters including  $\gamma_p$  and  $\sigma_p$  remain the same meanings as defined in the DPD formulation. All forces are truncated beyond a cutoff radius  $r_{c,p}$  that defines the length scale in the fluid–platelet contact region.<sup>17</sup>

The L–J force term  $\nabla U(r_{ij})$  helps the cytoskeleton-confined shapes and the incompressibility of platelets

against the applied shear stress of circumfluent plasma flow.<sup>64</sup> The dissipative and random force terms maintain the flow local thermodynamic and mechanical properties and exchange momentum to express interactions between the platelet and the flow particles. A no-slip boundary condition was applied at the fluid–membrane surface interface. A dissipative or drag force was added to enforce the no-slip boundary condition at the fluid and membrane interface, so that the fluid particles are dragged by the dissipative forces of the membrane particles as they are getting closer to the membrane surface, mimicking boundary layer mechanism where one layer drags its adjacent layers. The hard-core L–J force simultaneously provides a bounce-back reflection of fluid particles on the membrane (to prevent fluid particles from penetrating through the platelet membrane) with the no-slip achieved by slowing down the fluid particles (by the same repulsive term) as the fluid particles are getting closer to the membrane surface. The magnitude of the L–J force increases to infinity as the distance decreases, guaranteeing that the L–J force be strong enough to slow down and bounce back the fluid particles. The parameters for these forces were appropriately selected to preserve the dynamic properties of flowing platelets in shear viscous flows. This complex repulsive-drag force used to achieve the no-slip condition at the surface, was used to compute the values of the stresses on the surface of the membrane, following the force virial contribution using the algorithm in Refs. <sup>3,65,67</sup>.

The numerical solver is performed using LAMMPS.<sup>49</sup> The simulations employed the modified velocity–Verlet algorithm with  $\lambda = 0.5$ , which corresponds to the standard velocity–Verlet scheme widely used in molecular dynamics simulations.<sup>26</sup> Both CGMD and DPD propagate with the single step size  $\Delta t = 2 \times 10^{-4}$  in dimensionless units (i.e., 0.24 ns in SI units). The system was equilibrated with the choice of timescale. After the initial equilibrium, the same parameters and simulation procedures are used for the rigid and the deformable platelet models. The only difference is that one platelet model is deformable (Young’s modulus adjusted to experimental measurements) while the other is totally rigid. In addition, we monitored thermodynamic variables of the system for 10,000 timesteps: (1) total energy is  $E = 77.977 \pm 0.00054$  (mean  $\pm$  standard deviation) with deviation of 0.00069% (which is indeed negligible); (2) kinetic energy is  $Ke = 7.1663 \pm 0.0062$  with deviation of 0.087% (which is very small); (3) the flux of heat for the interface is  $7.92 \times 10^{-7} \pm 2.52 \times 10^{-6}$ ; and (4) the averaged kinetic energy per unit volume for the CGMD and DPD systems are  $1.640 \times 10^{-6} \pm 5.209 \times 10^{-9}$  and  $1.635 \times 10^{-6} \pm 1.430 \times 10^{-9}$ , respectively (the deviation between the two systems is

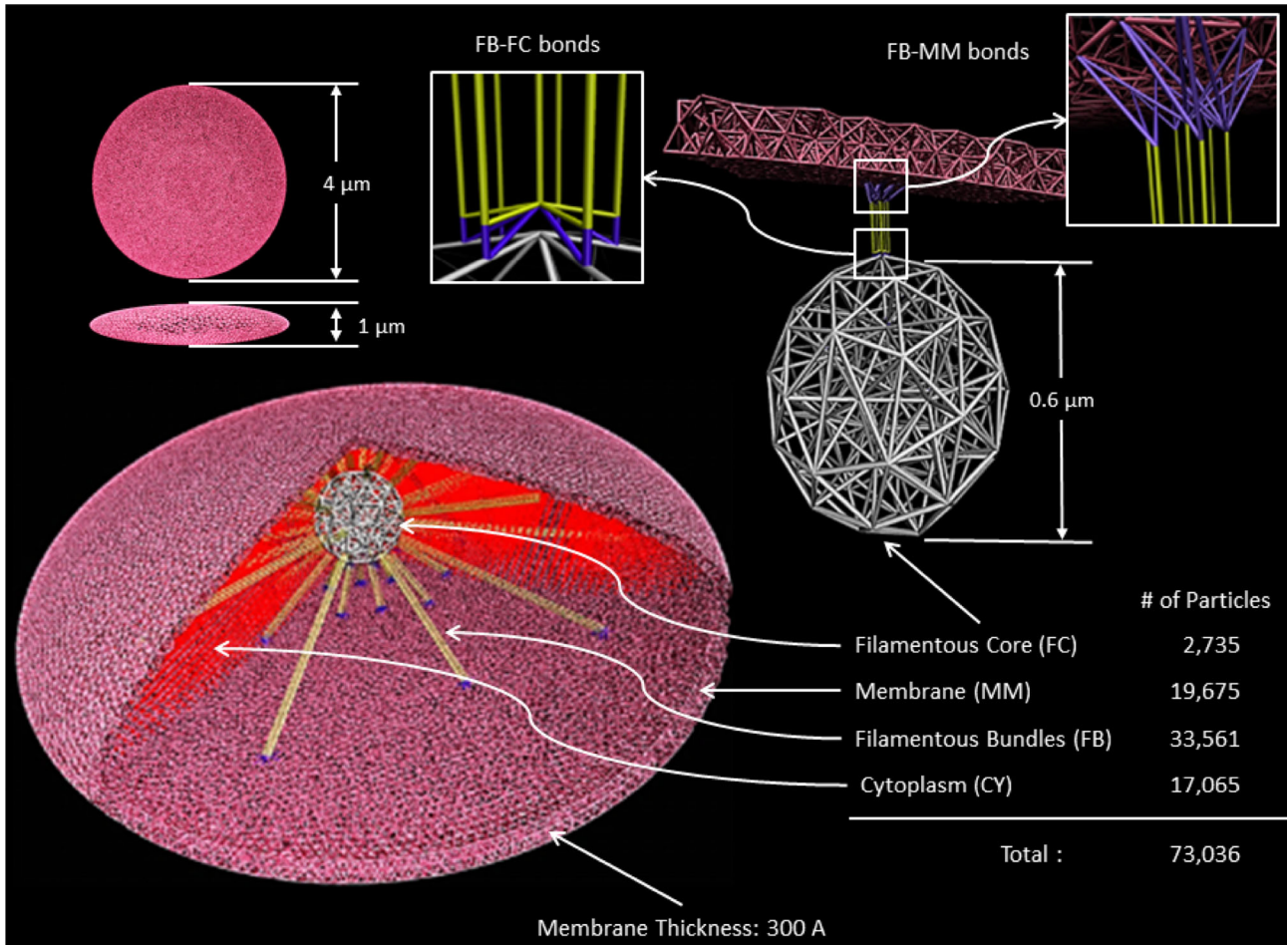
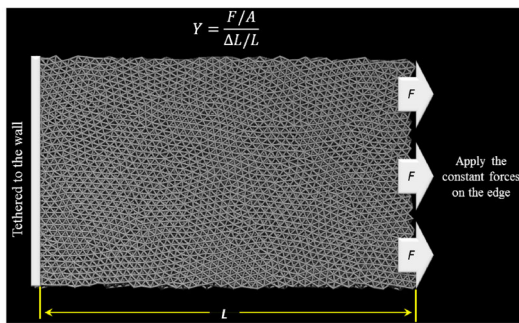


**FIGURE 4.** 3D geometry and internal components of the platelet model. It shows the geometry of the platelet on (upper left corner) detailed connections of FC with FC and MM particles (upper right corner). The filamentous core (FC) is a rigid core in the center of platelet. One end of the filamentous bundles (FB) is attached to the core and the other to the membrane. The cytoplasm (CY) filled the space between the membrane and the cytoskeleton.

**(a)** Schematic area-stretching experiment: one edge of the membrane is tethered to a fixed wall and the other edge is pulled by a constant force. Young's modulus is estimated using  $Y = (F/A)/(\Delta L/L)$ .  $F$  is the force exerted on the membrane,  $A$  is the cross-section area through which the force is applied,  $\Delta L$  is the amount by which the length of the membrane changes and  $L$  is the original length.



**(b)** Elastic responses of the membrane: the Young's modulus ( $\text{dyn cm}^{-2}$ ) vs. the applied force magnitude ( $\mu\text{N}$ )

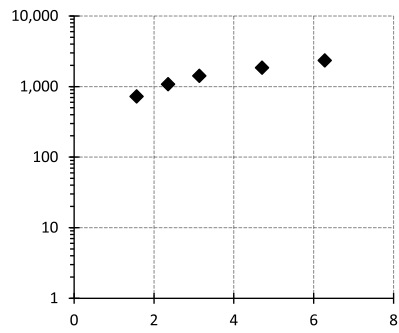


**FIGURE 5.** Schematic of the numerical stretching experiment (a) and elastic responses of the membranous system (b) using different stretching forces for assessing the Young's modulus of the deformable membrane model.

0.314%). The initial aspect ratio  $r_e = 0.25$  of the platelet model is changed to about 0.23 after immersion in flowing plasma.

Figure 6 shows the shapes of the rigid and the deformable models following the immersion. The rigid platelet model maintains the initial shape of the model which is an ideal ellipsoidal shape. The deformable model deforms according to the interactions between the deformable platelet model and the dynamic flow stresses around it. Structural integrity is fully maintained within certain degree of deformability. Numerically, we calculated the values of root mean square deviation (RMSD) for the shapes of deformable platelets (with and without flow). Calculation of RMSD is performed for the whole membrane system. The membrane structures of platelets without a fluid and in a fluid changed 0.08 and 2.43%, as compared to the initial shape. The numerical results demonstrated that: (1) without a fluid, the membrane of deformable platelets remains intact and very smooth (0.08% is very small) and (2) the surrounding flow stresses caused the deformable platelets to deform. In that, compression effect of springs in membrane is one observed microstructural change in deformable platelets and it is affected directly by the flow stresses. The shape of the deformable platelet model following the immersion in the fluid appears to offer a more realistic geometry of a platelet.

### Scaling of Model and Physical Units

Dimensionless constants and variables are often used in the DPD/CGMD models and they need to be scaled according to the physical units. The superscript \* denotes a quantity in the model dimensionless units while the physical units use the international system of units (SI Units). The subscript  $r$  denotes a reference unit used in the scaling scheme. The diameter of a real platelet is  $D_p = 4 \mu\text{m}$  and the diameter of a model platelet is  $D_p^* = 45$ . We defined the reference length scale  $\sigma_r$ , i.e., the model unit of length in SI, as  $\sigma_r = D_p / D_p^* \text{ m}$  where m stands for meter. The mass density of a blood fluid is  $\rho_f = 1060 \text{ kg/m}^3$  at 37 °C and the particle density of the DPD fluid is  $\rho_f^* = 3$ . We define the reference mass scale  $m_r$ , i.e., the model unit of mass in SI, as  $m_r = \rho_f \sigma^3 / \rho_f^* \text{ kg}$ . We define the reference velocity scale  $v_r$  as  $v_r = v_f / v_f^*$  where  $v_f^* = 4$  is the model velocity and  $v_f = 30 \text{ cm/s}$ . Hence, the reference time scale  $t_r$ , i.e., the time taken by the fluid particle to travel a reference length  $\sigma$ , is defined as  $t_r = \sigma / v_r \text{ s}$ , where s stands for seconds. According to the reference length, mass and time scales, the following dimensionless and physical units are introduced: the reference energy scale is  $e_r = m_r v_r^2$ . In the model dimensionless units, the shear rate  $\dot{\gamma}^*$ , shear stress  $\tau^*$  and viscosity  $\mu^*$  of the fluid

have  $\dot{\gamma}^* = 2v_f^*/D_f^*$  and  $\tau^* = \dot{\gamma}^* \cdot \mu^*$ .  $\mu^*$  is computed in the simulation. In SI units, the shear rate  $\dot{\gamma}$ , shear stress  $\tau$  and dynamics viscosity  $\mu$  of the fluid have  $\dot{\gamma} = 2v_f/D_f$ ,  $\tau = \tau^* \cdot e_r / \sigma_r^3$  and  $\mu = \tau / \dot{\gamma}$ . Reynolds number is  $Re = \rho_f v_u D_f / \mu_f$  where  $v_u$  is the mean velocity of the fluid,  $D_f$  is the diameter of the simulated flow region and  $\mu_f$  is the dynamic viscosity of the flow. Table 1 presents the scaling of model dimensionless units and physical units in the simulations.

## MULTISCALE CONSIDERATIONS

### *Spatiotemporal Averaging at Multiple Scales*

The goal of the multiscale framework is to investigate the microscopic shape changes of platelets under the macroscopic flow conditions and map the stress distribution on the surface membrane. Simulating the dynamic properties of the flowing platelets including the flipping orbits and the velocity contours on the membrane described above, facilitates dynamically accurate mapping of this stress distribution and is further used for comparing the stress accumulation when either a rigid or deformable platelet model is employed.

The multiscale model generates information at the microscopic level.<sup>49</sup> The conversion of this highly detailed information into top-scale is achieved using statistical mechanics.<sup>3,53</sup> The rigid model is a typical constrained system, in which the internal forces of constraint place the conditions on the positions in conjunction with their momenta.<sup>25</sup> Thus, though the rigid model is limited, in the absence of accurate measurements of the instantaneous quantities at the molecular level<sup>12</sup> it still provides a valuable reference point to assess the numerical results of the deformable model.<sup>60,76</sup> Nevertheless, directly comparing an unconstrained system (deformable platelet) with a constrained system (rigid platelet) is susceptible to the disparity in the degrees of freedom. To facilitate such comparison, a spatiotemporal averaging scheme was developed for the simulations at multiple scales. In this scheme, we consider an overwhelming number of interacting particles and compare the spatiotemporal-averaged effect of the deformable model with that of the prediction. Let  $\mathcal{A}$  be for the instantaneous value of some property and  $\Gamma$  for a particular point in phase space, then  $\mathcal{A}((t))$  evolves in time. Assume the experimental observable macroscopic property  $\mathcal{A}_{\text{obs}}$  be the time average of  $\mathcal{A}((t))$  taken over a long time interval<sup>3,54</sup>:

$$\mathcal{A}_{\text{obs}} = \langle \mathcal{A}((t)) \rangle_{\text{time}} \quad (5)$$

Appendix A describes the coarsening algorithms and compares the effects of various parameters settings.

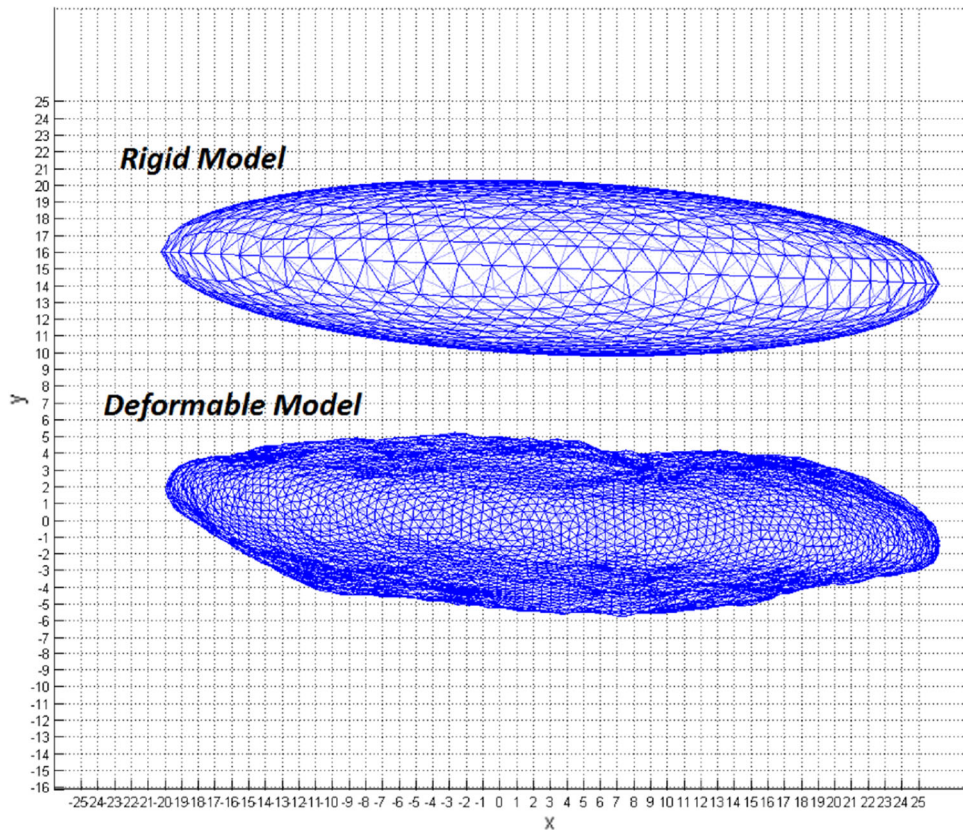


**FIGURE 6.** Shapes of the rigid and deformable platelet models following immersion in the plasma fluid.

**TABLE 1.** Reference units used in the DPD simulations; model parameters and translation of various input and output data from dimensionless to physical units.

Quantity	Symbols	Model values	SI values
Length	$\sigma_r$	1	88.89 nm
Mass	$m_r$	1	$2.48 \times 10^{-19}$ kg
Time	$t_r$	1	1.19 $\mu$ s
Energy	$\varepsilon_r$	1	$1.40 \times 10^{-21}$ kg m <sup>2</sup> /s <sup>2</sup>
Velocity	$v_r$	1	7.5 cm/s <sup>1</sup>
Diameter of microvessel	$D_f = \sigma_r D_f^*$	180	16 $\mu$ m
Diameter of the platelet	$D_p = \sigma_r D_p^*$	45	4 $\mu$ m
Thickness of the platelet		11.25	1 $\mu$ m
Aspect ratio of platelet	$r_e$	0.25	0.25
Mean velocity of the fluid	$v_u = v_u^*$	2	15 cm/s <sup>1</sup>
Shear rate	$\dot{\gamma} = \dot{\gamma}^* \cdot v_r / \sigma_r$	0.044	37,500 s <sup>-1</sup>
Shear stress	$\tau = \tau^* \cdot \varepsilon_r / \sigma_r^3$	18.56	369 dyne/cm <sup>2</sup>
Viscosity <sup>a</sup>	$\mu = \mu^* \cdot \varepsilon_r / v_r \sigma^2$	417.54	0.98 mPa s
Local Reynolds number <sup>b</sup>	$Re = \frac{\rho_l v_u^* D_f^*}{\mu_l} = \frac{\rho_l v_u D_f}{\mu_l}$	2.59	

<sup>a</sup>The normal value of plasma is 1.10–1.30 mPa s at 37 °C.<sup>34</sup>

<sup>b</sup>Typical Reynolds number range of blood flow in the body varies from 1 in small arterioles to approximately 4000 in the largest artery, the aorta.

At the nanoscale, the per-particle stress of particle  $p$  is expressed by a tensor  $\tau(p, t) = [\tau_{ij}]_{3 \times 3}$  where  $i$  and  $j$  take on values  $x, y, z$  to generate the six components of the symmetric tensor as it evolves in time. In MD simulation using several inter-atomic potentials, the

instantaneous stress tensor  $\tau(p, t)$  for particle  $p$  is expressed as<sup>29,49,65</sup>:

$$\tau_{ij} = - \left\{ mv_i v_j + \frac{1}{2} \sum_{n=1}^{N_p} (r_{1i} F_{1j} + r_{2i} F_{2j}) + \frac{1}{2} \sum_{m=1}^{N_b} (r_{1i} F_{1j} + r_{2i} F_{2j}) \right\} \quad (6)$$

**TABLE 2.** Schematic of the 4-staged parameterization on the interfacing potential. (Figure 8a through d that are referred to in the table show the impact of a specific variable on platelet-flipping dynamics.).

Stages\parameters	$\sigma_p$	$\varepsilon_p$	$\gamma_p$	$r_{c,p}$
Stage 1	Figure 8a	0.3	90	1.8
Stage 2	0.6	Figure 8b		
Stage 3		6.0	Figure 8c	
Stage 4			90	Figure 8d
Final values	0.6	6.0	90	1.6

$r_1$ ,  $r_2$  and  $F_1$  and  $F_2$  are the positions and resulting pairwise forces of the two particles. Here  $n$  loops over the  $N_p$  neighboring particles and  $m$  loops over the  $N_b$  bonded particles. The first term is the kinetic part and the last two terms are the potential part (springs and nonbonded). In the potential part, the nonbonded term describes membrane–fluid interactions and the bonded term (springs in membrane) is affected directly by the flow stresses. In Fig. 6 above, we compared RMSD of membrane of platelets without and with a fluid, illustrating that surrounding flows caused platelets to deform. Hence, these two parts are considered in the virial stress for equivalence with mechanical stresses.<sup>30,62</sup> There is no angle or other force terms in the membrane. The virial theorem routinely computes the volume averaged tensors for a collection of particles and thus the per-particle stress needs to be divided by a per-particle volume to have the unit of stress.<sup>29,65</sup> To implement the instantaneous stress tensor using the stress accumulation concept, the tensor is further rendered into a scalar value  $\hat{\tau}(p, t)$  using the following formulation<sup>1,6</sup>:

over the specified time period  $t$  produces the stress accumulation  $I(t)$ .

### Correlating Fluid–Platelet Interactions with Platelet-Flipping Dynamics

The hybrid potential (Eq. 4) allows us to describe the fluid–platelet interactions between two systems. This in turn requires establishing the parameters that will correlate with the platelet-flipping dynamics. Exhaustive search of the complete multiple-dimensional parameter space is the most reliable but computationally demanding method. It fails in practice due to its prohibitive computing requirements. An empirical multiple-staged search, e.g., a variable decoupling approach, is more feasible and was chosen accordingly. The first step in this search is to examine the impact of a specific unknown parameter on the target property, with all other parameters fixed. One unknown parameter is determined in each single stage. The parameters in former steps are used in the following steps, until all unknowns are established. Table 2 shows the schematic of a four-staged parameterization

$$\hat{\tau}(p, t) = \frac{1}{\sqrt{3}} \sqrt{\tau_{xx}^2 + \tau_{yy}^2 + \tau_{zz}^2 - \tau_{xx}\tau_{yy} - \tau_{xx}\tau_{zz} - \tau_{yy}\tau_{zz} + 3(\tau_{xy}^2 + \tau_{yz}^2 + \tau_{xz}^2)} \quad (7)$$

As described in Ref. 33 accumulation of the shear stress-exposure time product for period  $t$  for the membrane,  $I(t)$ , is calculated as:

$$I(t) = \sum_{i=1}^{n_t} \left( \frac{\sum_{k=1}^{N_m} \hat{\tau}(p_k, \Delta t_i)}{N_m} \right) \Delta t_i = \sum_{i=1}^{n_t} \langle \hat{\tau}(p, \Delta t_i) \rangle \cdot \Delta t_i \quad (8)$$

where  $\sum_{i=1}^{n_t} \Delta t_i = t$  and  $\langle \hat{\tau}(p, \Delta t_i) \rangle \equiv \left( \frac{\sum_{k=1}^{N_m} \hat{\tau}(p_k, \Delta t_i)}{N_m} \right)$

Here  $p_k$  represents one of  $N_m$  membrane particles and  $\hat{\tau}(p_k, \Delta t_i)$  is the scalar stress of particle  $p_k$  at time  $\Delta t_i$ .  $\langle \hat{\tau}(p, \Delta t_i) \rangle$  is the spatial-averaged stress across the particle-based membrane at time  $\Delta t_i$  and it represents the averaged effect of instantaneous per-particle stresses. Summing over products of  $\langle \hat{\tau}(p, \Delta t_i) \rangle$  and  $\Delta t_i$

for our hybrid potential. The initial values for stage 1 are empirical: the thermostat parameters  $\gamma_p$  and  $r_{c,p}$  are those used in the plasma domain and the conservative parameters  $\varepsilon_p$  and  $\sigma_p$  are those used in Ref. 17.

Numerical experiments were conducted to search the parameter space for maintaining the Jeffery’s orbits of spheroids in shear flows. The Jeffery’s orbits solution<sup>32,43</sup> describes the rotation of isolated ellipsoidal particles immersed in viscous shear flow and is widely used as a benchmark solution to parameterize and to validate numerical models of shear flows, e.g., Refs. 39,50,60,63. We use the Jeffery solution to parameterize the fluid–platelet friction interaction across the membrane.<sup>39,50,51,60</sup> In the parameterization, we consider Couette flow and platelet as an oblate spheroid

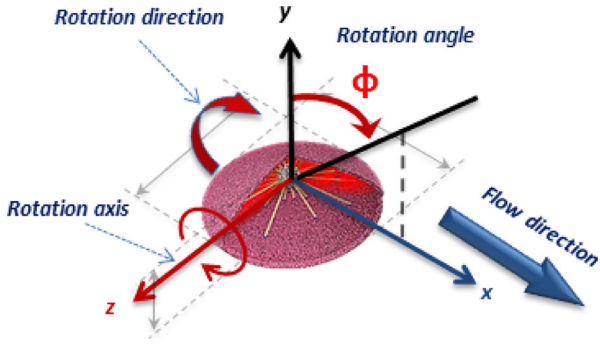


**FIGURE 7.** Coordinate system for platelet flipping.

(Fig. 1). The polar coordinate system used for the platelet flipping measurement is depicted in Fig. 7. We fix the inter-particle distances of intra-platelet cytoskeleton within a rigid body in order to correspond to a single ellipsoidal particle rotation in a simple shear flow.<sup>32</sup>

A series of parameter combinations were studied and compared to the Jeffrey's orbit solution, with deviations defined by an error function. In our simulations, the rotation angle  $\phi_s$  is assumed as a function of the total strain  $\dot{\gamma}t$  and the unknown model parameters:  $\phi_s = \phi_s(\dot{\gamma}t; \varepsilon_p, \sigma_p, \gamma_p, r_{c,p})$ . For clarity, the theoretical rotation angle function with respect to time is denoted as  $\phi_J = \phi(\dot{\gamma}t)$ . The subscripts s and J correspond to the simulation and the Jeffrey's solution respectively. Error function  $E(\dot{\gamma}t)$  is introduced to estimate the deviation of  $\phi_s$  compared to  $\phi_J$  over a half period, given by:

$$E(\dot{\gamma}t) = \int_0^{\pi(r_e + r_e^{-1})} \|\phi_s - \phi_J\| d(\dot{\gamma}t) \quad (9)$$

Equation (9) is evaluated by discretizing the time steps. The most suitable parameter combination was searched by minimizing the error function. The parameterization results and the effects of model parameters on the flipping behavior are described and discussed in the “Results” section.

## RESULTS

We first present the parameter sensitivity analysis based on the multiscale particle-based model for platelet-flipping dynamics, showing a sound parametric model. This is followed by a comparison of the particle-based simulation results with the Jeffrey's orbit solution, showing the differences between the simulation and the theory. We then investigate the effects

of the platelet-deforming mechanics on the platelet-flipping dynamics, identifying the differences and similarities between the rigid and deformable platelet models. In this investigation, we used exactly the same parameters and simulation procedures for the rigid and the deformable platelets. The only difference is that one platelet model is deformable (Young's modulus corresponding to experimental measurements) while the other is completely rigid. In addition, we investigate the dynamic stress distribution on the surface membrane of the platelets while flowing and flipping using the two models, depicting the differences in the stress distribution when deformability is ignored and ultimately the effect this may have on estimating the platelets activation potential.

### Parameter Sensitivity Analysis for the Platelet-Flipping Dynamics

The platelet dynamics definitely depend on every parameter but the parameter sensitivity varies widely. The platelet-flipping angle  $\phi(\dot{\gamma}t)$  is dictated by four parameters which collectively describe the fluid–platelet interactions. The impact of individual parameters on the platelet-flipping dynamics is widely diverse and their choice is also constrained by the coarsening scales. Figure 8 depicts the error functions  $E(\dot{\gamma}t)$  of a variety of model parameters at certain ranges and it shows that there is a clear dependency between the dynamics (flipping) and each of the parameters. In each of these experiments, one parameter is varied while all other three parameters are kept fixed. The results of this error analysis indicate that the equilibrium distance  $\sigma_p$  is the most sensitive parameter in determining the platelet-flipping dynamics and it also has to be constrained by the inter-particle distance of the surface membrane. Figure 8a indicates that a smaller  $\sigma_p$  always results in a better match with Jeffrey's orbits. However, a smaller  $\sigma_p$  greatly increases the possibility that a fluid particle may penetrate the membrane. It is observed that the blood plasma particles can easily penetrate the platelet when  $\sigma_p$  is less than 0.4. This is because the membrane, consisting of a finite collection of particles, may fail to prevent fluid particles from penetrating when the effective interaction range of the hybrid potential becomes considerably small. To avoid this penetration while still maintaining the flipping dynamics, we have selected  $\sigma_p = 0.6$ . Additionally, Fig. 8b shows an optimal value for the well depth parameter  $\varepsilon_p$ :  $\varepsilon_p = 6$ . Underestimating the value for  $\varepsilon_p$  constantly deteriorates the match with the Jeffrey's orbit solution. Combined with proper  $\sigma_p$ , increasing  $\varepsilon_p$  to an appropriate range, i.e., Refs. <sup>6,15</sup> improves the match. After the two conservative terms are determined, the

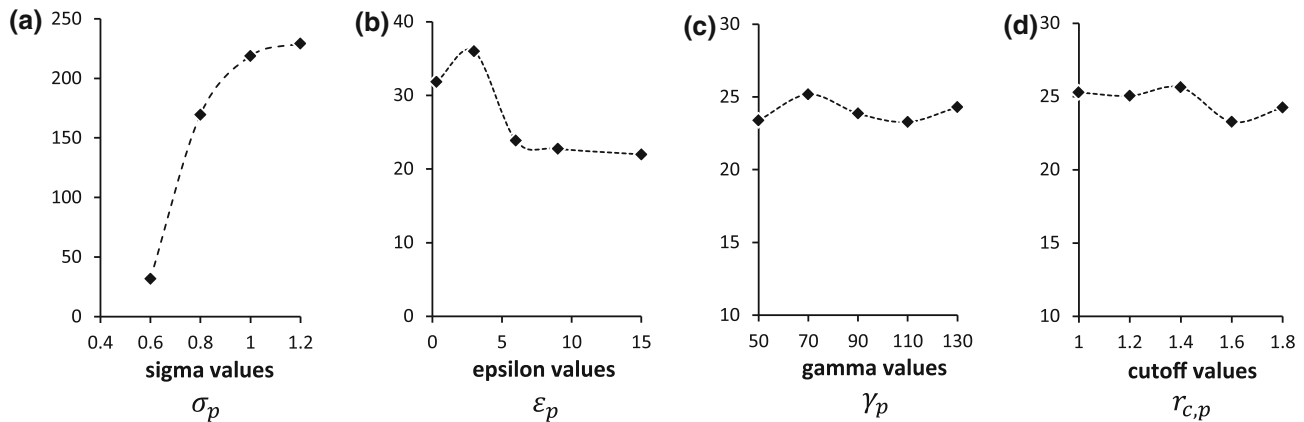


FIGURE 8. Error function  $E(\dot{\gamma}t)$  (y-axis) plotted vs. various parameters ( $\sigma_p$ ,  $\epsilon_p$ ,  $\gamma_p$  and  $r_{c,p}$ ) for platelets flipping in Couette flow.

thermostat term  $\gamma_p$  shows little impact on the platelet-flipping dynamics and thus  $\gamma_p = 90$  was kept unchanged. Similar procedure was applied to determine the cutoff term  $r_{c,p}$  in which  $r_{c,p} = 1.6$  was established as the best performer. Nevertheless, the thermostat terms influence the computing needs. A large  $r_{c,p}$  would cause a larger neighborhood and then a larger number of particles in the neighborhood of the surface membrane, leading to a substantial computing requirement between the fluid and membrane particle pairs. Compared to the conservative terms, the thermostat terms appear far less sensitive. The final values established for these parameters appear in Table 2.

#### Comparison of Particle-Based Simulation Results with Jeffery's Orbit Solution and the Effects of Platelet Deformability

We compare the multiscale particle-based simulation results with the solution of Jeffery's orbit in Couette flows. The comparison examines the angular velocities (Fig. 9), the angular acceleration (Fig. 10), and the rotation angle  $\phi(\dot{\gamma}t)$  (Fig. 11) vs. the total strain  $\dot{\gamma}t$ , with the predictions of the rigid and deformable platelet models. These results outline the degree to which the multiscale particle-based models agree with a benchmark analytical solution. Figures 9 and 10 reaffirm that the particle-based models had experienced the same stationary points as the Jeffery's orbit solution. Figure 11 shows flipping period that is consistent with the analytical solution. In the multiscale particle-based simulations, we consider a dynamic fluid–platelet interaction: once the particle based model is immersed in the fluid it adapts its shape accordingly (Fig. 6), followed by the surrounding fluid flow dynamically interacting with the platelet (Fig. 12), where the platelet further adapts its shape to the

dynamically changing flow-induced stresses (Fig. 13). The simulation results demonstrated that the platelet deformability would continuously influence the platelet's shape and the platelet-flipping dynamics. The rigid and deformable platelet models are compared in Figs. 6 and 13. Figure 6 shows the exterior shapes of the rigid and deformable platelet models after an initial flipping period. It clearly indicates that while the platelet loses its initial idealized oblate spheroid once immersed in the fluid, it can maintain the geometric skeleton when external stresses continue to be applied to it while flowing. This affirmed that the intra-platelet cytoplasm and the springy membrane were able to collectively provide a degree of incompressibility which was enough to resist the external pressure and maintain the platelet integrity.

Figure 13 depicts flipping velocity magnitude contours on the surface of the platelets. The deformability of platelets results in the observable difference in flipping motions such as rotation speeds. Specifically, at the early stages  $ts = 70$  and  $140 \mu\text{s}$ , the flow-induced shear stress dominates by dragging the platelet to spin about the z-axis. At this phase, the oblate spheroid shape is still maintained and the angular change of the deformable platelet is similar to that of the rigid model. As the flipping proceeds to  $ts = 210$  and  $280 \mu\text{s}$ , the spinning platelet continues to increase its surface area against the flow where the flow-induced normal stress dominates and contributes to accelerate the flipping. At this phase, the freely-moving membrane deforms such that the platelet reduces the flow-induced compression (by reducing the contact area). By the end of one flipping period ( $ts = 350 \mu\text{s}$ ), the platelet flattens back and restores the oblate spheroid shape—owing to the resilience of the spring-connected membrane. These dynamic complex shape changes that the platelet undergoes due to deformation or bending result in a

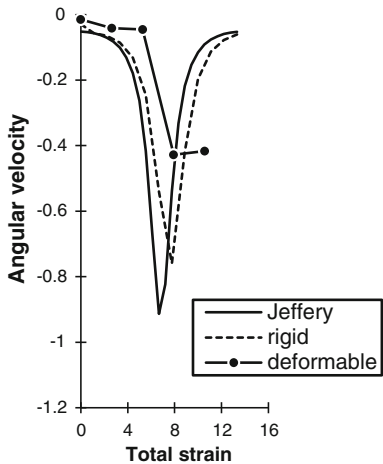


FIGURE 9. Angular velocity  $\dot{\phi}(\dot{\gamma}t)$  vs. the strain  $\dot{\gamma}t$  for Jeffery's orbit analytical solution and numerical solutions using the rigid and deformable platelet models.

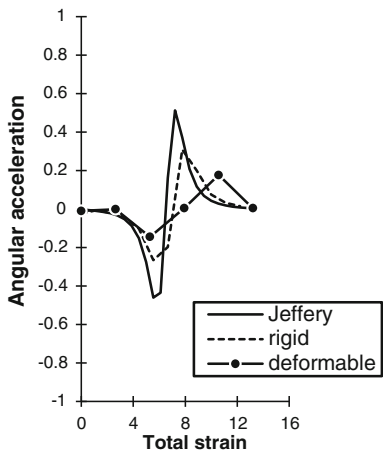


FIGURE 10. Angular acceleration  $\ddot{\phi}(\dot{\gamma}t)$  vs. the strain  $\dot{\gamma}t$  for Jeffery's orbit analytical solution and numerical solutions using the rigid and deformable platelet models.

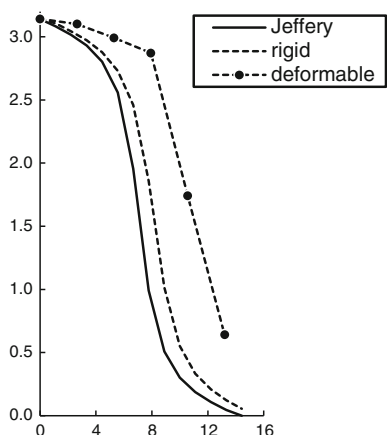
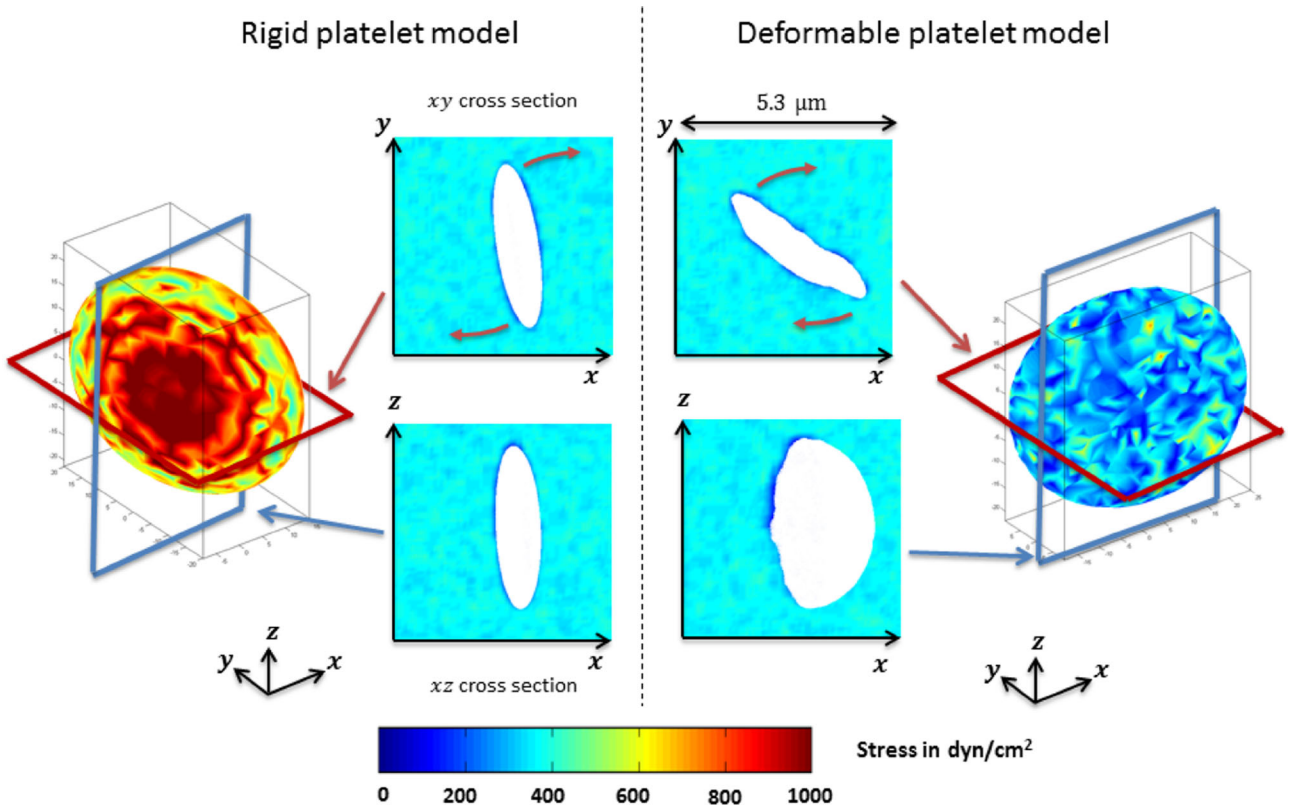


FIGURE 11. Rotation angles  $\phi(\dot{\gamma}t)$  vs. the total strain  $\dot{\gamma}t$  for the rigid and deformable platelet models as compared to Jeffery's orbit analytical solution in Couette flow.

slower flipping speed than that of the rigid model. The mechanical effects of the shear flows on the platelet deformation are also noticeable. In Fig. 13 (rigid model- top row), the rigidity constrains the ellipsoid at all times, resulting in no shape change. However, the membranous system of the deformable platelet (bottom row) continuously changes shapes owing to the flow-induced stresses, leading to the bending. These results clearly demonstrate that platelet stiffening directly influences the flow-induced platelet dynamics. This specific effect may be further studied to see if it may play a role in the effects of cortex stiffening occurring during platelets adhesion.<sup>38</sup>

#### Effects of Platelet Deformability on the Platelet Membrane Stress Distribution

Of primary concern from the mechanical point of view is the stress distribution on the platelet membrane surface, as this translates to the platelet activation potential. In our multiscale model, we show the contours of the stress magnitudes (in  $\text{dyn}/\text{cm}^2$ ) on the surface membrane for the rigid and deformable platelet models, in a 2D perspective (Fig. 14) and in 3D perspective (Fig. 15). Figure 12 shows a dynamic snapshot of the flow field stresses for the two models at  $t_s = 210 \mu\text{s}$ . The computation of the per-particle stresses uses Eqs. (6) and (7). The corresponding statistics of the particle-based flow-induced stresses (in  $\text{dyn cm}^{-2}$ ) on the membrane is presented in Fig. 16. This is followed by the stress accumulation results that are shown in Fig. 17. These results indicate that the flow-induced stresses in the rigid platelet model are on average approx. 2.6 times larger than those of the deformable model. The hydrodynamic stress will be less on deformable objects, as the surface will move and deform absorbing part of the external force. The spread of a stress distribution is measured as the standard deviation from the average value. Figure 16 clearly shows that the stress distribution of the deformable platelet tends to be less spread out compared to that of the rigid model. Figure 15 reaffirms this discovery by showing a clear high-stress area in the center of the rigid model but a more uniform distribution for the deformable model. Consequently, the accumulation of the flow-induced stresses on the membrane is different between the two models as shown in Fig. 17. Therefore, the rigidity of the platelet model is not a negligible factor when estimating flow-induced stresses on the platelets. The snapshot presented in Fig. 12 shows contours of the flow stress magnitudes, demonstrating that the rotation of the deformable platelet is influenced by the surrounding flowing particles in a similar manner as that of the rigid model.



**FIGURE 12.** A snapshot of the flow field stress magnitude contours for the rigid and deformable platelets in Couette flow ( $ts = 210 \mu s$ ).

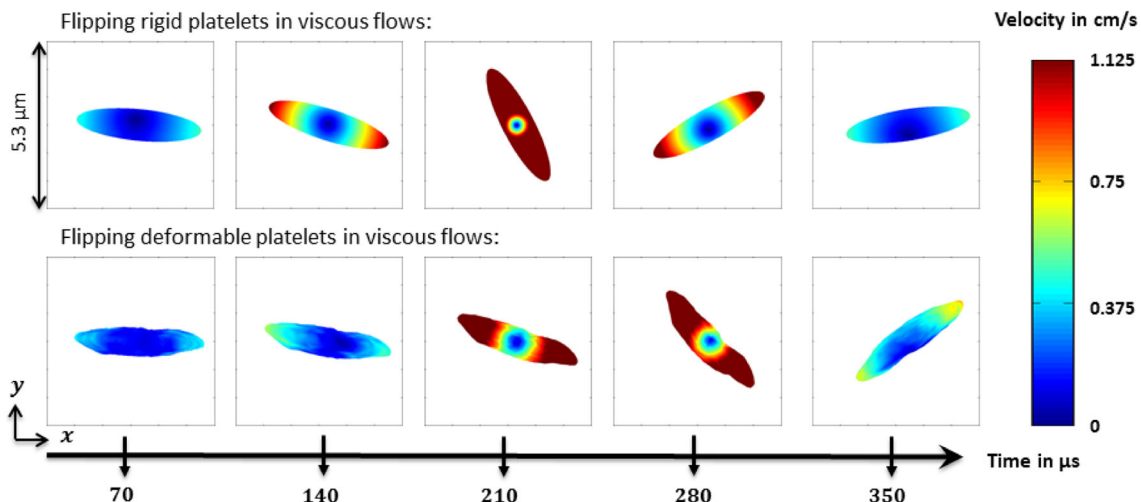


**FIGURE 13.** The 2D flipping velocity magnitude contours for the rigid and deformable platelets in Couette flow over time (color indicates the velocity magnitude in cm/s).

## DISCUSSION

The multiscale particle-based model described in this work integrates two levels of coarse-graining descriptions, DPD and CGMD, in a multiscale framework that yields the platelet-flipping dynamics in viscous shear flows and enables more accurate map-

ping of the stress distribution on the platelet membrane that may lead to its activation. The hybrid force field formulated between the DPD and CGMD systems offers an effective functional interface for the fluid–platelet interactions. The parameter sensitivity analysis describes an effective parameterization procedure that

enables the multiscale approach. The analysis further reiterates the importance of taking into account the platelet deformability for assessing more accurately the platelet activation potential.

From the parameter sensitivity analysis performed for the platelet-flipping dynamics, we conclude that a multi-dimensional parameter space in a complex multiscale model is required for estimating the sensitivity of the conservative parameters, followed by the thermostat terms which appear less sensitive to changes in their range. A length-scale-related parameter, including  $\sigma_p$  and  $r_{c,p}$ , needs to be further constrained by the coarsening level and the resulting computing require-

ments it may impose. In future studies, these empirical procedures can be applied to parameterize a similar multiscale system, instead of conducting an exhaustive search.

In describing the platelet-flipping dynamics, the multiscale particle-based model was able to yield flipping trajectories similar to those of the Jeffery's orbit solution. The results of a rigid platelet model are obviously closer to the analytical solution of a rigid spheroid in Couette flow than the classic Jeffery's orbit solution describes. However, although the Jeffery's orbit solution was used as a benchmark solution to platelet-flipping models,<sup>50,60,63</sup> its accuracy is limited: it

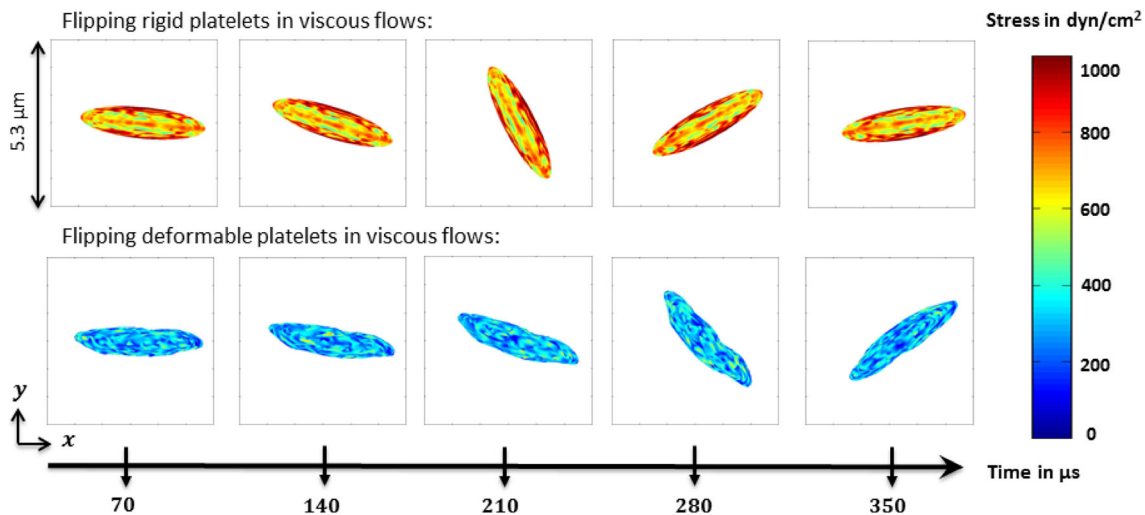


**FIGURE 14.** Membrane stress distribution—magnitude contours for the rigid and deformable platelets in Couette flow (xy-plane perspective, stress in  $\text{dyn}/\text{cm}^2$  and time in  $\mu\text{s}$ ).

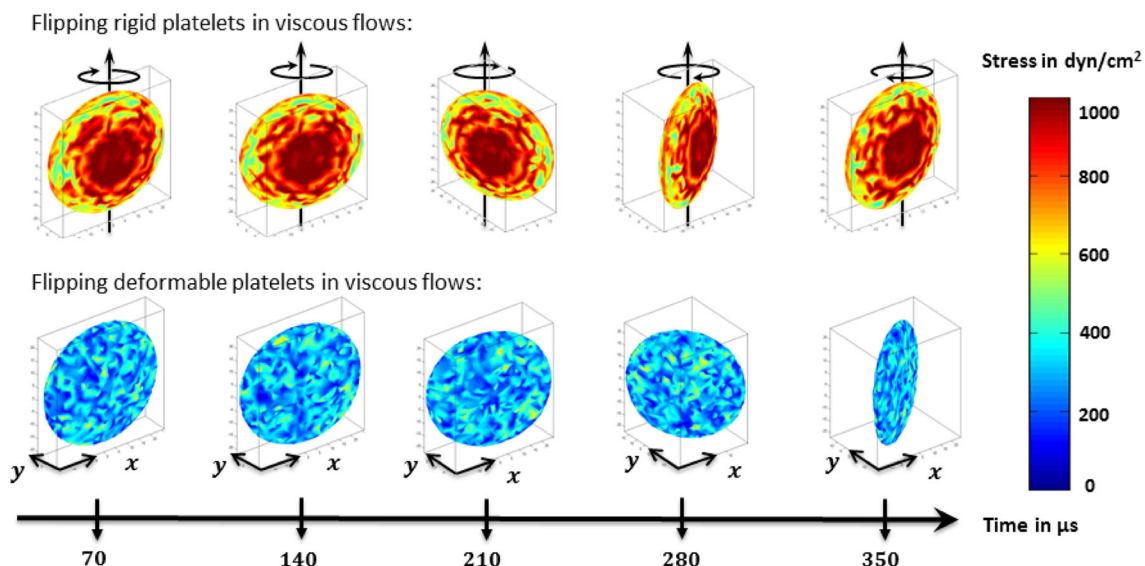


**FIGURE 15.** 3D membrane stress distribution—magnitude contours for the rigid and deformable platelets in Couette flow (3D perspective, stress in  $\text{dyn}/\text{cm}^2$  and time in  $\mu\text{s}$ ).

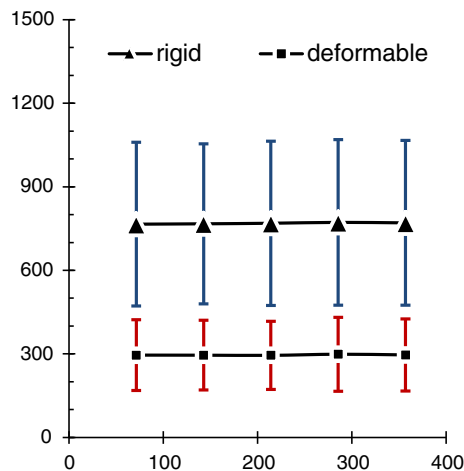


**FIGURE 16.** Average flow-induced stresses (y-axis in dyn/cm<sup>2</sup>) on the membrane over time (x-axis in µs) in Couette flow (error bars shows standard deviations.).

does not always agree with experimental results.<sup>63</sup> Jeffery's orbit does not consider the fluid-platelet dynamic interactions and the complex effects of platelet deformability. In addition, the deformable platelet model is a more realistic description of a flowing and flipping platelet, taking into account the dynamic fluid-platelet interactions and removing the idealized assumptions of the theoretical model. We observe that a particle-based simulation results may better reproduce the experimentally observed dynamics of flowing platelets. Probing more accurately the characteristics of the platelet-flipping dynamics requires modeling the systems at the micro and nano scales in a multiscale framework. Clearly at such length scales the platelet is not a rigid spheroid and the fluid flow may no longer be represented as a continuum, which is inherently assumed by theory. This, in turn, is bound to influence the prediction of the platelet activation potential.

The comparison between the particle-based simulation and the theory demonstrates the advantages of the multiscale modeling: the structural integrity (general oblate spheroid) of resting platelets was maintained and the ensuing microstructural changes were achieved within the constraints of feasible computational demands using available HPC resources. This considerable computational effort helps to bypass inherent challenges of multiscale multi-resolution phenomena.<sup>3,53</sup> In addition, the reproduction of a steady viscous laminar Couette flow was achieved with both the rigid and deformable models in all the numerical simulations performed. It demonstrates that the exchange of the flow's thermodynamical properties with the platelet system is a localized phenomenon that can still be conserved at the larger scales of the flow field. This result reaffirms the hypothesis that the dissipative and random force terms (thermostatting) of the hybrid potential is able to maintain the local ex-

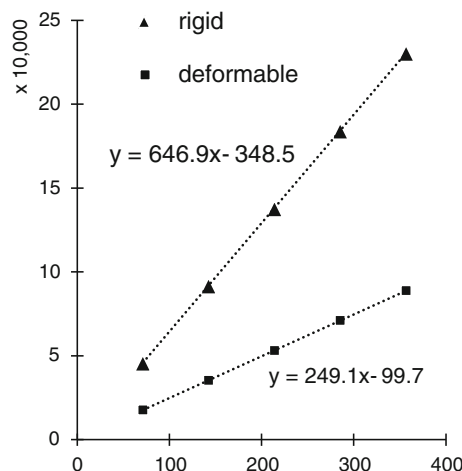


**FIGURE 17.** Accumulation of the shear stress-exposure time product (namely,  $I(t)$  for y-axis) on the rigid and deformable platelets over time (x-axis in µs) in Couette flow.

changes of energy in a flow field and further facilitate modeling fluid-platelet interactions.<sup>61</sup> The energy is dynamically transferred between the platelet and the flow as the rotational kinetic energy and angular momentum of the platelets smoothly change without irregularities or disruptions while the flowing platelets maintain their structural integrity. Another important aspect of platelet deformability involves the platelet activation potential. The overestimation of the stresses on the platelet membrane surface when a rigid platelet model is assumed additionally implies that the loss of the membranous elasticity disables the response of the microstructural changes within platelets and the way they react with the extracellular stimuli. The overestimation of the stresses may lead to prediction of premature platelet activation by the model. The overestimation of the dynamic stresses may be even greater in a more deformable platelet, as the elastic parameters of human platelets may vary within a considerable range (see Table 1 in Haga *et al.*<sup>27</sup>).

The particle-based simulation results demonstrated that the deformability of platelets could significantly influence the shear stress distribution on the platelet membrane. The rigid model platelet tends to over-estimate the stress magnitudes. In general, simplified models may yield erroneous estimations. For example, Yun *et al.*<sup>75</sup> compared the LBM-EBF and particle-tracking methods for estimating maximal shear stress on platelets in hinge flows of mechanical heart valves and found that the particle-tracking method would underestimate the stresses by 2.77–2.89 times. Clearly, a finer grained model is needed for predicting accurate results. Removing the rigidity constraint most current models assume could offer a far better estimation of flow-induced activation and its mechanism in, e.g., pathological flows in vessels<sup>4,58,59</sup> and platelets adhesion in which membrane stiffening plays a key role.<sup>7,38,46,70</sup> For

example, Martinez *et al.*<sup>38</sup> compared a rigid and deformable platelet attachment models and pointed out that “the results show that cortex stiffening significantly influences the force required for detachment as well as the cell-membrane internal stresses.” The rigidity assumption is usually applied to platelets because of their much higher stiffness as compared to that of RBCs. However, the results in this study clearly indicate that platelets should be treated with caution given the significant deformability shown in this simulation (which is also observed experimentally) that may lead to the overestimation of their activation potential. Conversely, the loss of normal membrane flexibility during adhesion because of stiffening<sup>7,38</sup> inevitably suggests that the mechanobiological processes involved needed to be taken into account by advanced models such as the multiscale particle model described in our study.

The platelet model includes the cytoskeleton which is missing from most current platelet models. Given their completely different physiological functions RBCs do not get activated like platelets do. Rapid and spontaneous cytoskeletal change is a major mechanism in the formation of pseudopodia during early platelet activation (actin filament extensions). Platelets deliver self-stimulating factors from internal components to the surface membrane, as well as expressing many receptors on the surface membrane (GPIb, GPIIb/IIIa, *etc.*)—all functions that RBCs do not perform. Hence, new platelet models are needed which depart from existing RBC models. Coupling an accurate dynamic stress distribution on the platelet surface with an internal cytoskeletal model can be used to trigger the cytoskeleton to undergo a dynamic change and form filopodia in response to flow induced shear stresses. Concurrently we continue to develop such a platelet model that facilitates dynamic filopod formation in response to various combinations of shear stress and exposure times. The much more accurate dynamic mapping of the stress distribution on the platelets membrane that is presented in the current paper will be integrated into this model, to predict both the location where a filopodia may be formed and to what extent it will grow. The model will be used to simulate the filopodia formation upon activation—maintaining the structural integrity (even with long filopods forming) and correlating to experiments where platelets are activated while getting exposed to various combinations of flow induced shear stress levels and durations.

## CONCLUSIONS

The mechanotransduction process of flow induced platelet activation in pathological blood flows plays a key role in platelet-mediated hemostasis and throm-

bosis. Quantitative mapping of these stresses on the surface membrane of platelets requires an effective multiscale approach that bridges the gap between the macroscopic flow scales and the mesoscopic scales characterizing this mechanotransduction process. A multiscale particle-based model that bridges these disparate scales was developed by integrating a top-scale DPD based flow model with a bottom-scale CGMD based platelet model which takes into account the microstructure of platelets. The model was applied to simulate fluid–platelet interaction phenomena such as platelets flipping in viscous shear flows and the ensuing stress distribution on the platelet model that may lead to platelet activation. A hybrid force field scheme was formulated for coupling the macroscopic thermostating and the microscopic conservative force terms. The fluid–platelet interaction between the two particle-based systems preserved the dynamic properties of the flowing platelets in viscous shear flows such as the flipping orbit, and the effects of platelet deformability on these dynamics was studied, as well as its activation potential by the flow induced stresses. The comparative study between rigid and deformable platelet models demonstrated that the deformable model preserved dynamic properties yet allowed the platelets to continuously change their morphology while reflecting the microstructural changes in response to these dynamic extracellular stresses. Although platelets deformability is far less than that of red blood cells, our study clearly demonstrates that the elastic deformation of platelets significantly influences the stress distribution on the surface membrane. Neglecting this may lead to an inaccurate prediction of the flow-induced platelet activation potential. To the best of our knowledge, the particle based multiscale DPD-CGMD methodology presented in our study is the first model for studying the fluid–platelet interaction between flowing deformable platelets and viscous blood plasma at multiple scales. It established a framework for multiscale modeling of flow induced platelet activation, including filopodia formation following activation, and may pave the way for studying similar phenomena of blood constituents under dynamic blood flow conditions.

## APPENDIX A: SPATIOTEMPORAL ANALYTICS AT MULTIPLE SCALES

### Methods

The instantaneous properties of the platelet constituent particles are measured in simulations and they are averaged over a period of time (referred to as the time-averaging technique) and then over a surface

volume (referred to as the space-averaging technique). The properties include the velocities and the stress tensors.

The temporal-averaging technique is to average a property  $\mathcal{A}$  among successive observations over a finite time interval and it is designed for demonstrating a common trend in that interval. Suppose that  $\mathcal{A}_i(0)$  is the initial velocity of a particle  $i$  and  $\{\mathcal{A}_i(j \cdot \delta t)\}_{j=0}^{\alpha-1}$  is a collection of  $\alpha$  successive points in time.  $i$  simply stands for an index of the particle. The time-averaged property  $\mathcal{A}_{i\text{time}}$  of the particle  $i$  in this interval is

$$\mathcal{A}_{i\text{time}} = \frac{1}{n} \sum_{j=0}^{\alpha-1} \mathcal{A}_i(j \cdot \delta t) \quad (10)$$

Here,  $\delta t$  is the length of time interval between two successive steps and it is always a multiple of the propagator in simulation.  $\alpha$  is the number of instantaneous observations in the succession. Naturally, a larger  $\alpha$  implies a more common trend in a longer time interval and the opposite extrema present a very instantaneous behavior.

The spatial-averaging technique is to average a property over a surface volume and it is specially designed for smoothing the spatial relevant fluctuations. Let the total membrane particles form a set of  $\{M_k(\mathbf{r}_k, \mathcal{A}_k)\}_{k=1}^K$  where  $\mathbf{r}_k$  and  $\mathcal{A}_k$  are the position and property of a particle  $k$ . For convenience, we introduce the set notations: the  $\delta$ -neighborhood of a point positioned at  $\mathbf{p}$  is denoted as  $D(\mathbf{p}, \delta)$  where  $\delta$  is a positive number. A point positioned at  $\mathbf{q}$  is said within  $D(\mathbf{p}, \delta)$  if  $\|\mathbf{p} - \mathbf{q}\|_2 \leq \delta$  and denoted as  $\mathbf{q} \in D(\mathbf{p}, \delta)$ . The intersection  $D(\mathbf{p}, \delta) \cap \{M_k\}$  is the set that contains all of the membrane particles that are also within the  $\delta$ -neighborhood of point  $\mathbf{p}$ .  $\phi$  is an empty set.  $|\mathcal{A}|$  is the number of elements in a set  $\mathcal{A}$ .

The space-averaging technique involves two steps:

Step 1: Generate a collection of lattices  $\{L_i(p_i, \bar{\mathcal{A}}_i)\}_{i=1}^\beta$

where  $\mathbf{p}_i$  and  $\bar{\mathcal{A}}_i$  are the position and unknown property associated with lattice  $L_i$ .  $\beta = |L_i|$  is the total number of lattices and the bar stands for the spatial relevant averaging. The collection of lattices forms the coverage of the entire platelet surface if and only if it satisfies: for each  $\mathbf{r}_k$ , there is a  $D(\mathbf{p}_i, \delta)$  such that  $\mathbf{r}_k \in D(\mathbf{p}_i, \delta)$  and  $D(\mathbf{p}_i, \delta) \cap \{\mathbf{r}_k\} \neq \phi$  for any  $i$ .

Step 2: Calculate the property  $\mathcal{A}_i$  for lattice  $L_i$  as

$$\bar{\mathcal{A}}_i = \frac{1}{\omega_i} \sum_{\mathbf{r}_k \in D(\mathbf{p}_i, \delta)} \mathcal{A}_k \quad (11)$$

Here  $\omega_i = |D(\mathbf{p}_i, \delta) \cap \{\mathbf{r}_k\}| \geq 1$  and  $\delta$  depends on the average distance of the nearest lattices.

In total, the temporal and spatial averaging techniques form the multiscale analytic scheme and the attention is paid to the consistency between the observed property  $\mathcal{A}_{obs}$  and the spatiotemporal-averaged property  $\bar{\mathcal{A}}_{time}$ .

$$\mathcal{A}_{obs} \cong \overline{\mathcal{A}_{time}} \quad (12)$$

### Configurations

We consider four coarsening configurations (Table A1) for the space-averaging technique. The figures are ordered from the finest to the coarsest grained levels.

### Results

Figure A1 shows the effects of temporal averaging on the platelet-flipping velocity magnitudes. In the legend, “nanosecond” means that we calculate the average magnitude of flipping velocities of the

**TABLE A1. Different collections of lattices for the space-averaging technique.**

Original		Lattices		
Total of points ( $\beta$ )	19,675 particles	9800 points	4800 points	1350 points
Ratio of points over original particles (%)	100	49.8	24.4	6.86

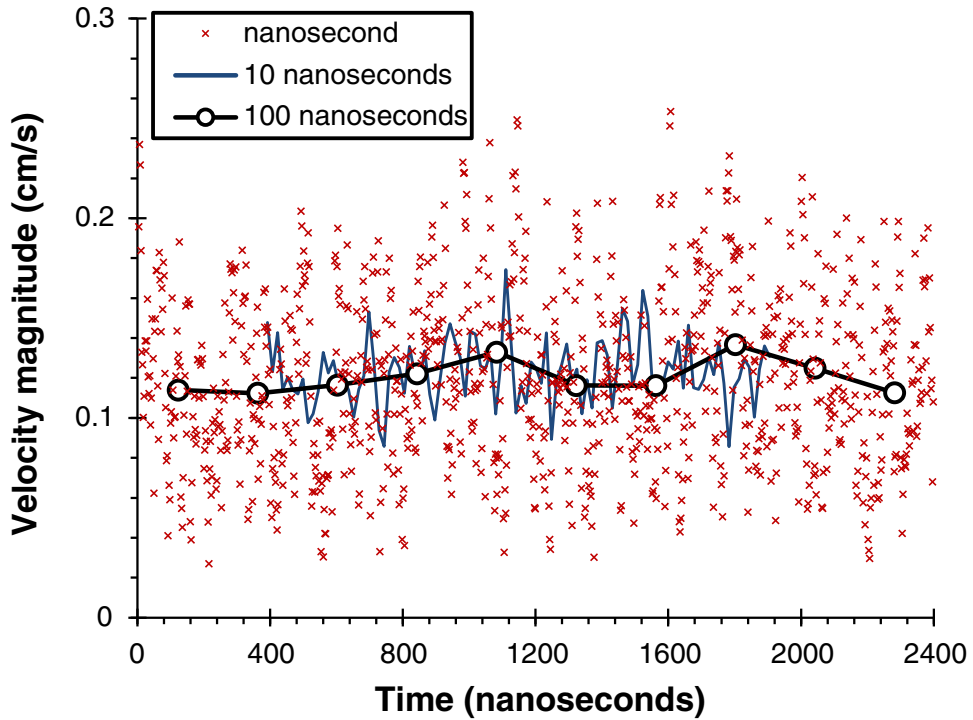


FIGURE A1. The effect of temporal averaging on the flipping velocity magnitude.

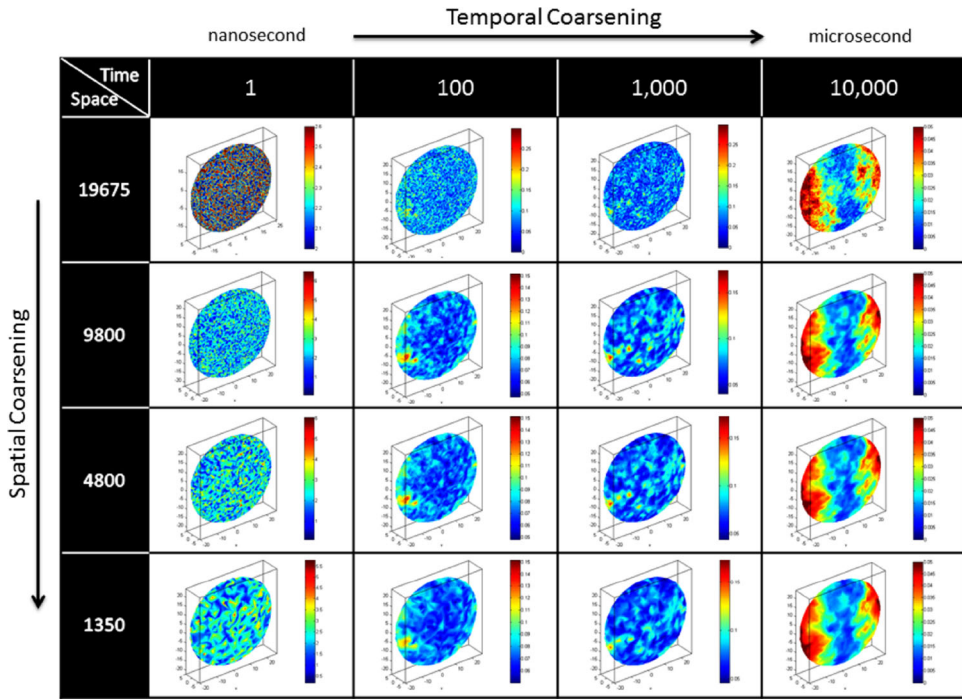
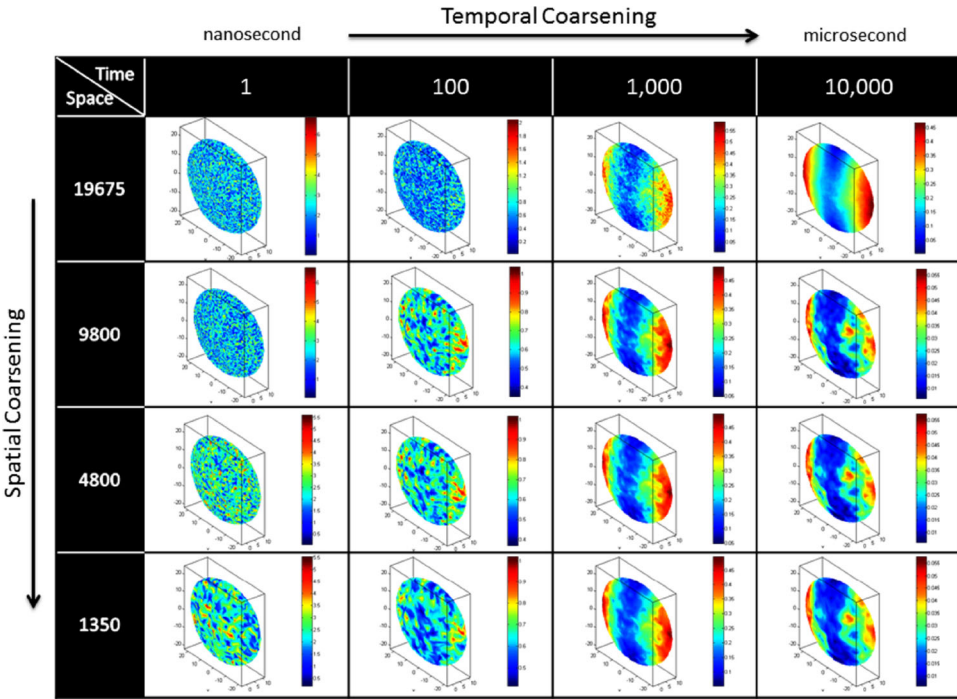


FIGURE A2. The velocity profiles of the case using different coarsening parameters ( $ts = 60$ ).

membranous particles every nanosecond (ns). Similarly, “10 ns” and “100 ns” mean the same calculations are performed every 10 and 100 ns, respectively. This figure illustrates the obvious disparity of the fluctua-

tions of numeric values at varied temporal coarse-graining scales. For example, the instantaneous values at the very microscopic level showed the most flickering. Second, the microscopic values of the membrane



**FIGURE A3.** The velocity profiles of the case using different coarsening parameters ( $ts = 240$ ).

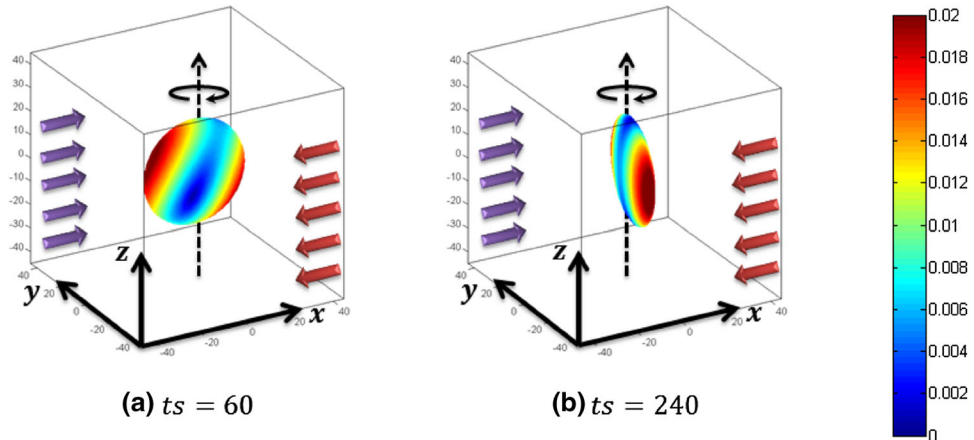


**FIGURE A4.** The velocity profiles of the rigid platelet model at ( $ts = 60$ ) and ( $ts = 240$ ).

system at varied temporal scales characterized the same macroscopic quality: the long-term trends. The spatiotemporal averaging technique is a useful method to convert microscopic information to macroscopic qualities for the multiscale modeling and demonstrate a clearer resolution for long-term observables.

Different combinations of temporal and spatial coarse graining parameters would represent the same metadata with multiple-resolutions. Figures A2 and A3 present the analytic results for  $ts = 60$  and 240 (dimensionless time) respectively. These results re-verify that the instantaneous velocity profile fluctuates

very rapidly thanks to the high-frequency oscillations of the massive membrane particles and the profile becomes smoother as the instantaneous velocities are processed by the time-averaging and space-averaging techniques. A rigid platelet model is an extreme case of the coarsening as shown in Fig. A4. We observe that the velocity profile of a deformable model more resembles that of a rigid model, as the temporal coarsening method continues to a larger temporal scale. For instance, both of the models show the consistent phenomena that the high-velocity areas occur merely on the flipping edges while the central stripe has

a relatively small flipping rate. Additionally, the spatial coarsening method characterized the “flickering” membrane fluctuations in certain degree, without using the very many particles. For example in Figs. A2 and A3,  $\beta = 1350$  (bottom right subplot) renders the similar profile as using  $\beta = 19,675$  (top right subplot), in particular at  $\alpha = 10,000$  (last columns).

Collectively, the results demonstrate: the rigid platelet model never can reflect the molecular-scale fluctuations of natural membranes owing to the complete stiffness. At the opposite extreme, an atomistic-scale simulation provides over detailed access to the spectrum of thermal fluctuations but its application demands the computing power. As a trade-off, the multiscale model does not only reflect the thermal fluctuations of the platelet particles but also maintains the computational feasibility.

## ACKNOWLEDGMENTS

This publication was made possible by Grants from the National Institute of Health: NHLBI R21 HL096930-01A2 (DB) and NIBIB Quantum Award Implementation Phase II-U01 EB012487-0 (DB). This research utilized the HPC resource Sunway BlueLight MPP cluster at the National Supercomputing Center in Jinan, China.

## CONFLICT OF INTEREST

Peng Zhang, Chao Gao, Na Zhang, Marvin J. Slepian, Yuefan Deng, and Danny Bluestein declare that they have no conflicts of interest.

## ETHICAL STANDARDS

No human studies were carried out by the authors for this article. No animal studies were carried out by the authors for this article.

## REFERENCES

- <sup>1</sup>Alemu, Y., and D. Bluestein. Flow-induced platelet activation and damage accumulation in a mechanical heart valve: numerical studies. *Artif. Organs* 31:677–688, 2007.
- <sup>2</sup>Alemu, Y., G. Girdhar, M. Xenos, J. Sheriff, J. Jesty, S. Einav, and D. Bluestein. Design optimization of a mechanical heart valve for reducing valve thrombogenicity—a case study with ATS valve. *ASAIO J.* 56:389–396, 2010.
- <sup>3</sup>Allen, M. P., and D. J. Tildesley. Computer Simulation of Liquids. Oxford: Clarendon Press, 1989.
- <sup>4</sup>AlMomani, T., H. S. Udaykumar, J. S. Marshall, and K. B. Chandran. Micro-scale dynamic simulation of erythrocyte–platelet interaction in blood flow. *Ann. Biomed. Eng.* 36:905–920, 2008.
- <sup>5</sup>Alsheikh-Ali, A. A., G. D. Kitsios, E. M. Balk, J. Lau, and S. Ip. The vulnerable atherosclerotic plaque: scope of the literature. *Ann. Intern. Med.* 153:387–395, 2010.
- <sup>6</sup>Apel, J., R. Paul, S. Klaus, T. Siess, and H. Reul. Assessment of hemolysis related quantities in a microaxial blood pump by computational fluid dynamics. *Artif. Organs* 25:341–347, 2001.
- <sup>7</sup>Avrahami, I., and M. Gharib. Effects of membrane stiffening on focal-adhesion bonding under steady and unsteady conditions. Bio Micro and Nanosystems Conference, 2006. BMN’06: IEEE; 2006, p. 85.
- <sup>8</sup>Bluestein, D., Y. Alemu, I. Avrahami, M. Gharib, K. Dumont, J. J. Ricotta, and S. Einav. Influence of microcalcifications on vulnerable plaque mechanics using FSI modeling. *J. Biomech.* 41:1111–1118, 2008.
- <sup>9</sup>Bluestein, D., W. Yin, K. Affeld, and J. Jesty. Flow-induced platelet activation in mechanical heart valves. *J. Heart Valve Dis.* 13:501–508, 2004.
- <sup>10</sup>Chee, C. Y., H. P. Lee, and C. Lu. Using 3D fluid–structure interaction model to analyse the biomechanical properties of erythrocyte. *Phys. Lett. A* 372:1357–1362, 2008.
- <sup>11</sup>Deng, Y., P. Zhang, C. Marques, R. Powell, and L. Zhang. Analysis of Linpack and power efficiencies of the world’s TOP500 supercomputers. *Parallel Comput.* 39:271–279, 2013.
- <sup>12</sup>Dror, R. O., R. M. Dirks, J. P. Grossman, H. Xu, and D. E. Shaw. Biomolecular simulation: a computational microscope for molecular biology. *Annu. Rev. Biophys.* 41:429–452, 2012.
- <sup>13</sup>Espanol, P., and P. Warren. Statistical mechanics of dissipative particle dynamics. *EPL (Europhysics Letters)* 30:191, 1995.
- <sup>14</sup>Fedosov, D. A., B. Caswell, and G. E. Karniadakis. A multiscale red blood cell model with accurate mechanics, rheology, and dynamics. *Biophys. J.* 98:2215–2225, 2010.
- <sup>15</sup>Fedosov, D. A., B. Caswell, A. S. Popel, and G. E. Karniadakis. Blood flow and cell-free layer in microvessels. *Microcirculation* 17:615–628, 2010.
- <sup>16</sup>Fedosov, D. A., M. Dao, G. E. Karniadakis, and S. Suresh. Computational biorheology of human blood flow in health and disease. *Ann. Biomed. Eng.* 42:368–387, 2014.
- <sup>17</sup>Fedosov, D. A., and G. E. Karniadakis. Triple-decker: Interfacing atomistic–mesoscopic–continuum flow regimes. *J. Comput. Phys.* 228:1157–1171, 2009.
- <sup>18</sup>Fedosov, D. A., H. Lei, B. Caswell, S. Suresh, and G. E. Karniadakis. Multiscale modeling of red blood cell mechanics and blood flow in malaria. *PLoS Comput. Biol.* 7:e1002270, 2011.
- <sup>19</sup>Fedosov, D. A., W. Pan, B. Caswell, G. Gompper, and G. E. Karniadakis. Predicting human blood viscosity in silico. *Proc. Natl. Acad. Sci. USA* 108:11772–11777, 2011.
- <sup>20</sup>Fedosov, D. A., I. V. Pivkin, and G. E. Karniadakis. Velocity limit in DPD simulations of wall-bounded flows. *J. Comput. Phys.* 227:2540–2559, 2008.
- <sup>21</sup>Feng, R., M. Xenos, G. Girdhar, W. Kang, J. W. Davenport, Y. F. Deng, and D. Bluestein. Viscous flow simulation in a stenosis model using discrete particle dynamics: a comparison between DPD and CFD. *Biomech. Model. Mechanobiol.* 11:119–129, 2012.
- <sup>22</sup>Filipovic, N., M. Kojic, and A. Tsuda. Modelling thrombosis using dissipative particle dynamics method. *Philos. Trans. R. Soc. A* 366:3265–3279, 2008.
- <sup>23</sup>Filipovic, N., D. Ravnic, M. Kojic, S. J. Mentzer, S. Haber, and A. Tsuda. Interactions of blood cell constituents: experimental investigation and computational modeling by

- discrete particle dynamics algorithm. *Microvasc. Res.* 75:279–284, 2008.
- <sup>24</sup>Frojmovic, M. M., and J. G. Milton. Human platelet size, shape, and related functions in health and disease. *Physiol. Rev.* 62:185–261, 1982.
- <sup>25</sup>Goldstein, H. Classical mechanics (2nd ed.). Reading, MA: Addison-Wesley Pub. Co., 1980.
- <sup>26</sup>Groot, R., and P. Warren. Dissipative particle dynamics: bridging the gap between atomistic and mesoscopic simulation. *J. Chem. Phys.* 107:4423–4435, 1997.
- <sup>27</sup>Haga, J. H., A. J. Beaudoin, J. G. White, and J. Strony. Quantification of the passive mechanical properties of the resting platelet. *Ann. Biomed. Eng.* 26:268–277, 1998.
- <sup>28</sup>Hartwig, J. H., and M. Desisto. The cytoskeleton of the resting human blood–Platelet—structure of the membrane skeleton and its attachment to actin-filaments. *J. Cell Biol.* 112:407–425, 1991.
- <sup>29</sup>Heinz, H., W. Paul, and K. Binder. Calculation of local pressure tensors in systems with many-body interactions. *Phys. Rev. E* 72:066704, 2005.
- <sup>30</sup>Hoover, W. G., C. G. Hoover, and J. F. Lutsko. Microscopic and macroscopic stress with gravitational and rotational forces. *Phys. Rev. E* 79:036709, 2009.
- <sup>31</sup>Ishiyama, T., K. Nitadori, and J. Makino. 4.45 Pflops astrophysical N-body simulation on K computer: the gravitational trillion-body problem. Proceedings of the International Conference on High Performance Computing, Networking, Storage and Analysis. Salt Lake City, UT: IEEE Computer Society Press; 2012, pp. 1–10.
- <sup>32</sup>Jeffery, G. B. The motion of ellipsoidal particles in a viscous fluid. *Proc. R. Soc. Lond. Ser. A Contain. Pap. Math. Phys. Character* 102:161–179, 1922.
- <sup>33</sup>Jesty, J., W. Yin, P. Perrotta, and D. Bluestein. Platelet activation in a circulating flow loop: combined effects of shear stress and exposure time. *Platelets* 14:143–149, 2003.
- <sup>34</sup>Kesmarky, G., P. Kenyeres, M. Rabai, and K. Toth. Plasma viscosity: a forgotten variable. *Clin. Hemorheol. Microcirc.* 39:243–246, 2008.
- <sup>35</sup>Kroll, M. H., J. D. Hellums, L. V. McIntire, A. I. Schafer, and J. L. Moake. Platelets and shear stress. *Blood* 88:1525–1541, 1996.
- <sup>36</sup>Lees, A., and S. Edwards. The computer study of transport processes under extreme conditions. *J. Phys. C* 5:1921, 1972.
- <sup>37</sup>Lei, H., D. A. Fedosov, and G. E. Karniadakis. Time-dependent and outflow boundary conditions for Dissipative Particle Dynamics. *J. Comput. Phys.* 230:3765–3779, 2011.
- <sup>38</sup>Martinez, E. J., Y. Lanir, and S. Einav. Effects of contact-induced membrane stiffening on platelet adhesion. *Bio-mech. Model. Mechanobiol.* 2:157–167, 2004.
- <sup>39</sup>Mody, N. A., and M. R. King. Three-dimensional simulations of a platelet-shaped spheroid near a wall in shear flow. *Phys. Fluids* 17:113302-1–113302-12, 2005.
- <sup>40</sup>Mody, N. A., and M. R. King. Platelet adhesive dynamics. Part I: Characterization of platelet hydrodynamic collisions and wall effects. *Biophys. J.* 95:2539–2555, 2008.
- <sup>41</sup>Mody, N. A., and M. R. King. Platelet adhesive dynamics. Part II: High shear-induced transient aggregation via GPIbalpha-vWF-GPIbalpha bridging. *Biophys. J.* 95:2556–2574, 2008.
- <sup>42</sup>Mody, N. A., O. Lomakin, T. A. Doggett, T. G. Diacovo, and M. R. King. Mechanics of transient platelet adhesion to von Willebrand factor under flow. *Biophys. J.* 88:1432–1443, 2005.
- <sup>43</sup>Moses, K. B., S. G. Advani, and A. Reinhardt. Investigation of fiber motion near solid boundaries in simple shear flow. *Rheol. Acta* 40:296–306, 2001.
- <sup>44</sup>O'Brien, J. R., and G. P. Salmon. An independent haemostatic mechanism: shear induced platelet aggregation. *Adv. Exp. Med. Biol.* 281:287–296, 1990.
- <sup>45</sup>Padding, J. T., and W. J. Briels. Systematic coarse-graining of the dynamics of entangled polymer melts: the road from chemistry to rheology. *J. Phys. Condens. Matter* 23:233101, 2011.
- <sup>46</sup>Pasqua, A., L. Maibaum, G. Oster, D. A. Fletcher, and P. L. Geissler. Large-scale simulations of fluctuating biological membranes. *J. Chem. Phys.* 132:154107, 2010.
- <sup>47</sup>Pivkin, I. V., and G. E. Karniadakis. A new method to impose no-slip boundary conditions in dissipative particle dynamics. *J. Comput. Phys.* 207:114–128, 2005.
- <sup>48</sup>Pivkin, I. V., and G. E. Karniadakis. Accurate coarse-grained modeling of red blood cells. *Phys. Rev. Lett.* 101:118105, 2008.
- <sup>49</sup>Plimpton, S., A. Thompson, and P. Crozier. LAMMPS Molecular Dynamics Simulator. 2014. <http://lammps.sandia.gov/>.
- <sup>50</sup>Pozrikidis, C. Flipping of an adherent blood platelet over a substrate. *J. Fluid Mech.* 568:161–172, 2006.
- <sup>51</sup>Ramanujan, S., and C. Pozrikidis. Deformation of liquid capsules enclosed by elastic membranes in simple shear flow: large deformations and the effect of fluid viscosities. *J. Fluid Mech.* 361:117–143, 1998.
- <sup>52</sup>Rambhia, S. H., X. Liang, M. Xenos, Y. Alemu, N. Maldonado, A. Kelly, S. Chakraborti, S. Weinbaum, L. Cardoso, S. Einav, and D. Bluestein. Microcalcifications increase coronary vulnerable plaque rupture potential: a patient-based micro-CT fluid–structure interaction study. *Ann. Biomed. Eng.* 40:1443–1454, 2012.
- <sup>53</sup>Reichl, L. E. A Modern Course in Statistical Physics. Austin: University of Texas Press, 1980.
- <sup>54</sup>Reichl, L. E., and I. Prigogine. A Modern Course in Statistical Physics. Austin: University of Texas press, 1980.
- <sup>55</sup>Revenga, M., I. Zuniga, P. Espanol, and I. Pagonabarraga. Boundary models in DPD. *Int. J. Mod. Phys. C* 9:1319–1328, 1998.
- <sup>56</sup>Riniker, S., J. R. Allison, and W. F. van Gunsteren. On developing coarse-grained models for biomolecular simulation: a review. *Phys. Chem. Chem. Phys.* 14:12423–12430, 2012.
- <sup>57</sup>Rossinelli, D., B. Hejazialhosseini, P. Hadjidoukas, C. Bekas, A. Curioni, A. Bertsch, S. Futral, S. J. Schmidt, N. A. Adams, and P. Koumoutsakos. 11 PFLOP/s simulations of cloud cavitation collapse. Proceedings of SC13: International Conference for High Performance Computing, Networking, Storage and Analysis. Denver, Colorado: ACM; 2013, pp. 1–13.
- <sup>58</sup>Sheriff, J., D. Bluestein, G. Girdhar, and J. Jesty. High-shear stress sensitizes platelets to subsequent low-shear conditions. *Ann. Biomed. Eng.* 38:1442–1450, 2010.
- <sup>59</sup>Sheriff, J., J. S. Soares, M. Xenos, J. Jesty, M. J. Slepian, and D. Bluestein. Evaluation of shear-induced platelet activation models under constant and dynamic shear stress loading conditions relevant to devices. *Ann. Biomed. Eng.* 41:1279–1296, 2013.
- <sup>60</sup>Soares, J. S., C. Gao, Y. Alemu, M. Slepian, and D. Bluestein. Simulation of platelets suspension flowing through a stenosis model using a dissipative particle dynamics approach. *Ann. Biomed. Eng.* 41:2318–2333, 2013.

- <sup>61</sup>Soddeemann, T., B. Dünweg, and K. Kremer. Dissipative particle dynamics: a useful thermostat for equilibrium and nonequilibrium molecular dynamics simulations. *Phys. Rev. E* 68:046702, 2003.
- <sup>62</sup>Subramaniyan, A. K., and C. T. Sun. Continuum interpretation of viral stress in molecular simulations. *Int. J. Solids Struct.* 45:4340–4346, 2008.
- <sup>63</sup>Sweet, C. R., S. Chatterjee, Z. Xu, K. Bisordi, E. D. Rosen, and M. Alber. Modelling platelet–blood flow interaction using the subcellular element Langevin method. *J. R. Soc. Interface* 8:1760–1771, 2011.
- <sup>64</sup>Symeonidis, V., and G. E. Karniadakis. A family of time-staggered schemes for integrating hybrid DPD models for polymers: algorithms and applications. *J. Comput. Phys.* 218:82–101, 2006.
- <sup>65</sup>Thompson, A. P., S. J. Plimpton, and W. Mattson. General formulation of pressure and stress tensor for arbitrary many-body interaction potentials under periodic boundary conditions. *J. Chem. Phys.* 131:154107, 2009.
- <sup>66</sup>Tosenberger, A., F. Ataullakhhanov, N. Bessonov, M. Panteleev, A. Tokarev, and V. Volpert. Modelling of thrombus growth and growth stop in flow by the method of dissipative particle dynamics. *Russ. J. Numer. Anal. Math. Model.* 27:507–522, 2012.
- <sup>67</sup>Tuckerman, M. Statistical Mechanics and Molecular Simulations. Oxford: Oxford University Press, 2008.
- <sup>68</sup>Visser, D. C., H. C. J. Hoefsloot, and P. D. Iedema. Modelling multi-viscosity systems with dissipative particle dynamics. *J. Comput. Phys.* 214:491–504, 2006.
- <sup>69</sup>Wang, N. T., and A. L. Fogelson. Computational methods for continuum models of platelet aggregation. *J. Comput. Phys.* 151:649–675, 1999.
- <sup>70</sup>Ward, M. D., and D. A. Hammer. A theoretical analysis for the effect of focal contact formation on cell-substrate attachment strength. *Biophys. J.* 64:936–959, 1993.
- <sup>71</sup>Willemse, S. M., H. C. J. Hoefsloot, and P. D. Iedema. No-slip boundary condition in dissipative particle dynamics. *Int. J. Mod. Phys. C* 11:881–890, 2000.
- <sup>72</sup>Xenos, M., G. Girdhar, Y. Alemu, J. Jesty, M. Slepian, S. Einav, and D. Bluestein. Device thrombogenicity emulator (DTE)—design optimization methodology for cardiovascular devices: a study in two bileaflet MHV designs. *J. Biomech.* 43:2400–2409, 2010.
- <sup>73</sup>Yamaguchi, T., T. Ishikawa, Y. Imai, N. Matsuki, M. Xenos, Y. F. Deng, and D. Bluestein. Particle-based methods for multiscale modeling of blood flow in the circulation and in devices: challenges and future directions. *Ann. Biomed. Eng.* 38:1225–1235, 2010.
- <sup>74</sup>Yin, W., Y. Alemu, K. Affeld, J. Jesty, and D. Bluestein. Flow-induced platelet activation in bileaflet and mono-leaflet mechanical heart valves. *Ann. Biomed. Eng.* 32:1058–1066, 2004.
- <sup>75</sup>Yun, B. M., J. Wu, H. A. Simon, S. Arjunon, F. Sotiropoulos, C. K. Aidun, and A. P. Yoganathan. A numerical investigation of blood damage in the hinge area of aortic bileaflet mechanical heart valves during the leakage phase. *Ann. Biomed. Eng.* 40:1468–1485, 2012.
- <sup>76</sup>Zhang, D. D., D. E. Smith, D. A. Jack, and S. Montgomery-Smith. Numerical evaluation of single fiber motion for short-fiber-reinforced composite materials processing. *J. Manuf. Sci. Eng. Trans. ASME* 133:051002–051009, 2011.
- <sup>77</sup>Zhang, N., P. Zhang, W. Kang, D. Bluestein, and Y. F. Deng. Parameterizing the Morse potential for coarse-grained modeling of blood plasma. *J. Comput. Phys.* 257:726–736, 2014.